Stress intensity factors and T-stresses by boundary integral equations: 3D statics

J.J. Yang[1], J.Z. Liu[2*], J. Sladek[3], V. Sladek[3] and P.H. Wen[4*]

[1] *School of Traffic and Transportation Engineering, Changsha University of Science and Technology, China*

[2] *School of Mathematics, Physics and Energy Engineering, Hunan Institute of Technology, China*

[3] *Institute of Construction and Architecture, Slovak Academy of Sciences, 84503 Bratislava, Slovakia*

[4] *School of Engineering and Materials Science, Queen Mary, University of London, London, UK, E1 4NS*

Abstract

This paper presents the boundary integral equation method (BIEM) for the stress intensity factors and elasticity *T*-stresses evaluation in 3D problems. Flat rectangular, elliptic, penny-shaped cracks and rectangular crack on a cylindrical surface have been investigated. The hyper-singular integrals are treated with the Taylor's series expansion of the kernel, and the Chebyshev polynomials of the second kind are used to solve the integral equations numerically. The stress intensity factors (SIFs) on the crack front are obtained by the coefficients of the Chebyshev polynomials. In order to verify the solutions by BIEM, the finite element method (FEM) with ABAQUS is conducted. The efficiency and convergence of the BIEM are observed in three examples. Comparisons are made with the analytical solutions in the stress intensity factor handbook and numerical solutions using the displacement discontinuity method (DDM).

Key words: Boundary integral equation method, Taylor's series expansion, Chebyshev polynomials interpolation, stress intensity factor, *T*-stress.

* Corresponding author's email: hnhyls@126.com (Liu); p.h.wen@qmul.ac.uk (Wen)

1. Introduction

The second term in the Williams (1957) series expansion for linear elastic crack-tip fields, called *T*-stress, has found many applications in linear and elastoplastic fracture mechanics. This is because the *T*-stress has certain effects on the crack growth direction, the shape and size of the plastic zone, the crack-tip constraint and the fracture toughness by Du and Hancock [1], Larsson and Carlson [2], and O'Dowd et al. [3] in the early stage. It was showed that the sign of the *T*-stress determines the stability of a straight model path by Cotterell and Rice [4]. A comprehensive overview of past research on the *T*-stress was presented by Gupta et al [5] and Fett [6]. These recent studies indicate that the value of the elastic *T*-stress, along with the *J*-integral or other measure of the scale of crack-tip deformation, can provide exceptional improvement in the ability to describe local crack-tip stress triaxiality on the scale of fracture process zone concluded by Nakamura and Parks in [7]. The *T*-stress arises in the discussions of crack stability of extension for linear elastic materials. A straight crack path has been shown to be stable when $T<0$ for small amounts of crack growth under opening mode, whereas the path will be unstable and, therefore, will deviate from being straight when $T>0$. Furthermore, the *T*-stress plays an important role in elastic-plastic fracture analysis. The early study observed that the *T*-stress can have a significant effect on the plastic zone size and shape, and that the small plastic zones in actual specimens can be predicted adequately by including the *T*-stress as a second crack-tip parameter.

The FEM is a mature, well-developed and most widely used in engineering in both linear and non-linear problems including the evaluation of the stress intensity factors and *T*-stress, see Nakamura and Parks in [7,8]. However, the fine element mesh should be used to obtain accurate T-stresses at crack tip front and special treatment of stress singularity should be introduced for both two and three dimensional problems. Apart from the FEM, the boundary element method (BEM) based on the integral equation fundamentals in elastostatics is one of the most efficient tools to deal with the same problems which can be traced back to classical mathematical formulations by Betti [9], Somigliana [10], Muskhelishvili [11] and Kupradze [12]. In 1960s, the development of these formulations in the context of numerical methods was subsequently developed by Massonnet [13]. Rizzo [14] and Cruse [15] introduced the first formulation for three-dimensional elasticity. A single region technique for the crack growth analysis, call the dual boundary element method (DBEM), was formulated by Hong and Chen [16,17] in 1988 and

implemented by Portela et al [18] in 1990s for two-dimensional and by Mi and Aliabadi [19] for three-dimensional problems. If the displacement equation is applied on one of the crack surfaces and the traction equation on the other, a general mixed-mode fracture problems can be solved with a single-region formulation. One of the advantages of DBEM is that the crack extension procedure can be modelled easily by adding extra elements. General review of the DBEM can be found in [20] by Aliabadi and [21] by Chen respectively.

The displacement discontinuity method (DDM) is a type of boundary integral method wherein the fundamental solution used is the displacement due to a constant displacement discontinuity on a finite segment in an infinite or semi-infinite elastic medium. Boundary value problems in mechanics are solved by distributing a series of such displacement discontinuity segments over a boundary on which the displacement or stress is known. The solution is found by adjusting the magnitude of each displacement discontinuity to match the boundary conditions. Hyper singular boundary integral equation to 2D/3D elastodynamics, anisotropic medium and Reissner's plate bending problems with cracks has been widely used in the solid engineering. A general review of DDM can be found in Ref. [22] by Wen et al. It was firstly reported by Crouch [23] in the geomechanics and solid mechanics. The DDM was extended to static/dynamic 2D/3D fracture mechanics by Wen et al in [24-26] with great success in 1990's. The M-integral technique along with BEM and an auxiliary solution, Sladek et al. [27-29] shown that it was effective for 2D thermoelastic stress, elastodynamic stress and the interfaces between dissimilar materials. For 2D elastostatics and elastodynamics, the finite block method by Wen [30], Li et al [31] Huang et al [32] combined with the stress and displacement fields of the Williams' series [33] (static) and the Deng's series [34] (dynamic) was developed to evaluate the SIFs, *T*-stress and other coefficients for the rest of the regular terms in the stress fields precisely. Similar to SIFs, the values of *T*-stress strongly depend on the relative crack length, geometry and Poisson's ratio. It is interesting that the *T*-stress for 2D problem is independent of material property and on the contrary they are influenced by the Poisson's ratio of the material in the three-dimensional cases. Although several numerical/analytical methods have been developed to calculate *T*-stresses, the solutions for 3D cracked specimens are very limited [35,36,37]. Penny-shaped crack embedded in an infinite body subjected to a remote tension and bending loading conditions represents bench mark for the cracked components in engineering by Wang [38].

Although the hyper singular integral equation method such a DDM is mature and well developed in fracture mechanics, high accurate solutions of stress intensity factors and T-stress are required as benchmarks in numerical engineering. The T-stresses in front of 2D curved surface cracks tips are observed firstly in this present paper with both analytical and numerical solutions. The numerical approach based on the boundary integral equations for three dimensional problems are presented to evaluate the SIFs and *T*-stresses for a curved surface crack in an infinite body. The Chebyshev polynomials of the second kind are employed in the numerical procedure, and the hyper-singular integrals are treated using the Taylor's series expansion. The convergence is observed with increasing numbers of the collocation point and comparison is made with either analytical solutions from the stress intensity factor handbook or numerical solutions by 3D FEM and DDM.

2. T-stresses in three-dimensions

2.1. *Mode-I crack front solutions*

In mixed mode fracture isotropic elasticity, the leading terms in a series expansion of the stress field near the crack front are described [1] as

$$\begin{aligned}
\sigma_{11} &= \frac{K_{\mathrm{I}}}{\sqrt{2\pi r}}\cos\frac{\theta}{2}\left(1-\sin\frac{\theta}{2}\sin\frac{3\theta}{2}\right)-\frac{K_{\mathrm{II}}}{\sqrt{2\pi r}}\sin\frac{\theta}{2}\left(2+\cos\frac{\theta}{2}\cos\frac{3\theta}{2}\right)+T_{11}+O(r^{1/2}),\\
\sigma_{22} &= 2\nu\left[\frac{K_{\mathrm{I}}}{\sqrt{2\pi r}}\cos\frac{\theta}{2}-\frac{K_{\mathrm{II}}}{\sqrt{2\pi r}}\sin\frac{\theta}{2}\right]+T_{22}+O(r^{1/2}),\\
\sigma_{33} &= \frac{K_{\mathrm{I}}}{\sqrt{2\pi r}}\cos\frac{\theta}{2}\left(1+\sin\frac{\theta}{2}\sin\frac{3\theta}{2}\right)+\frac{K_{\mathrm{II}}}{\sqrt{2\pi r}}\sin\frac{\theta}{2}\cos\frac{\theta}{2}\cos\frac{3\theta}{2}+O(r^{1/2}),\\
\sigma_{13} &= \frac{K_{\mathrm{I}}}{\sqrt{2\pi r}}\sin\frac{\theta}{2}\cos\frac{\theta}{2}\cos\frac{3\theta}{2}-\frac{K_{\mathrm{II}}}{\sqrt{2\pi r}}\cos\frac{\theta}{2}\left(1-\sin\frac{\theta}{2}\sin\frac{3\theta}{2}\right)+O(r^{1/2}),\\
\sigma_{12} &= -\frac{K_{\mathrm{III}}}{\sqrt{2\pi r}}\sin\frac{\theta}{2}+T_{12}+O(r^{1/2}),\\
\sigma_{23} &= \frac{K_{\mathrm{III}}}{\sqrt{2\pi r}}\cos\frac{\theta}{2}+O(r^{1/2}),
\end{aligned} \tag{1}$$

and the displacement fields give

$$u_1 = \frac{1+\nu}{E}\sqrt{\frac{2r}{\pi}}\left\{K_{\mathrm{I}}\cos\frac{\theta}{2}\left[(1-2\nu)+\sin^2\frac{\theta}{2}\right]+K_{\mathrm{II}}\sin\frac{\theta}{2}\left[2(1-\nu)+\cos^2\frac{\theta}{2}\right]\right\}+O(r),$$
$$u_2 = \frac{2(1+\nu)}{E}\sqrt{\frac{2r}{\pi}}K_{\mathrm{III}}\sin\frac{\theta}{2}+O(r), \qquad (2)$$
$$u_3 = \frac{1+\nu}{E}\sqrt{\frac{2r}{\pi}}\left\{K_{\mathrm{I}}\sin\frac{\theta}{2}\left[2(1-\nu)-\cos^2\frac{\theta}{2}\right]-K_{\mathrm{II}}\cos\frac{\theta}{2}\left[(1-2\nu)-\sin^2\frac{\theta}{2}\right]\right\}+O(r),$$

where the subscripts 1, 2 and 3 indicate a local Cartesian coordinate system (x_1 direction is formed by the intersection of the plane normal to the crack front and the plane tangential to the crack surface; x_2 direction is tangential to the crack front, and x_3 direction is orthogonal to the crack surface), r and θ are the polar coordinates coordinates of the plane normal to the crack front, K_{I}, K_{II} and K_{III} represent the modes I, II and III stress intensity factors, E and ν are the Young's modulus and the Poisson's ratio respectively. T_{11}, T_{22} and T_{12} in Eq. (1) are T-stresses parallel to the crack surface. In case of a flat crack, it is lying in plane $x_1 - x_2$ of the global Cartesian coordinate system.

2.2. *Boundary integral equation for 2D crack in an infinite body*

The mathematical difficulties associated with the application of the displacement boundary integral equation to modelling crack problems (degeneracy of two crack faces into one surface in un-deformed state) have been described by Cruse [15]. Recall that Somigliana's identity [10] for displacements at an interior point $\boldsymbol{\xi}$ is given, in the absence of a body force, by

$$u_i(\boldsymbol{\xi}) = \int_S U_{ij}^*(\boldsymbol{\xi},\mathbf{x})t_j(\mathbf{x})dS - \int_S T_{ij}^*(\boldsymbol{\xi},\mathbf{x})u_j(\mathbf{x})dS \qquad i,j=1,2,3, \qquad (3)$$

where $U_{ij}^*(\boldsymbol{\xi},\mathbf{x})$ and $T_{ij}^*(\boldsymbol{\xi},\mathbf{x})$ are fundamental solutions of displacement and traction, $\boldsymbol{\xi}\in V, \mathbf{x}\in S$, V denotes the domain with boundary S of the problem, for three dimensional body. Considering a curved surface crack embedded in an infinite body, as $U_{ij}^*(\boldsymbol{\xi},\mathbf{x}^+) = U_{ij}^*(\boldsymbol{\xi},\mathbf{x}^-)$, $T_{ij}^*(\boldsymbol{\xi},\mathbf{x}^+) = -T_{ij}^*(\boldsymbol{\xi},\mathbf{x}^-)$, Eq. (3) becomes

$$u_i(\boldsymbol{\xi}) = \int_{S^-} U_{ij}^*(\boldsymbol{\xi},\mathbf{x})\Sigma t_j(\mathbf{x})dS - \int_{S^-} T_{ij}^*(\boldsymbol{\xi},\mathbf{x})\Delta u_j(\mathbf{x})dS \qquad i,j=1,2,3, \qquad (4)$$

where S^- denotes the crack lower surface, $\Sigma t_j(\boldsymbol{\xi}) = t_j^+ + t_j^-$, $\Delta u_j(\boldsymbol{\xi}) = u_j^+ - u_j^-$. For traction free crack, or when the crack is subjected to opposite tractions ($\Sigma t_j(\boldsymbol{\xi}) = 0$), we have

$$u_i(\boldsymbol{\xi}) = -\int_{S^-} T_{ij}^*(\boldsymbol{\xi}, \mathbf{x}) \Delta u_j(\mathbf{x}) dS \qquad i, j = 1,2,3 . \tag{5}$$

By using Hook's law, the stress integral equation becomes

$$\sigma_{ij}(\boldsymbol{\xi}) = -\int_{S^-} S_{ijk}^*(\boldsymbol{\xi}, \mathbf{x}) \Delta u_k(\mathbf{x}) dS . \tag{6}$$

If the collocation point $\boldsymbol{\xi}^-$ lies on the crack surface S^-, we have [39]

$$\frac{1}{2}\sigma_{ij}(\boldsymbol{\xi}^-) + \frac{1}{2}\sigma_{ij}(\boldsymbol{\xi}^+) = -\oint_{S^-} S_{ijk}^*(\boldsymbol{\xi}^-, \mathbf{x}) \Delta u_k(\mathbf{x}) dS , \tag{7}$$

where $\oint$ indicates the Hadamard principal value integral [17], and the integral function [39] results

$$\begin{aligned} S_{ijk}^*(\boldsymbol{\xi}^-, \mathbf{x}) = \frac{E}{8\pi(1-\nu^2)r^3} \Big\{ & 3\frac{\partial r}{\partial n}\left[(1-2\nu)\delta_{ij}r_{,k} + \nu(\delta_{ik}r_{,j} + \delta_{jk}r_{,i}) - 5r_{,i}r_{,j}r_{,k}\right] \\ & + 3\nu(n_i r_{,j} r_{,k} + n_j r_{,i} r_{,k}) + (1-2\nu)(3n_k r_{,i} r_{,j} + n_j\delta_{ik} + n_i\delta_{jk}) - (1-4\nu)n_k\delta_{ij} \Big\}, \end{aligned} \tag{8}$$

in which $r = \left|\boldsymbol{\xi}^- - \mathbf{x}\right|$, $r_{,i}$ denotes differentiation with respect to x_i, δ_{ij} is the Kronecker delta, n_i indicates the outward unit normal and $\partial r / \partial n = r_{,i} n_i$. Multiplying the above equation by the outward unit normal $n_j(\boldsymbol{\xi}^-)$ and noting that $n_j(\boldsymbol{\xi}^-) = -n_j(\boldsymbol{\xi}^+)$ results following traction boundary integral

$$\frac{1}{2}t_i(\boldsymbol{\xi}^-) - \frac{1}{2}t_i(\boldsymbol{\xi}^+) = -n_j(\boldsymbol{\xi}^-)\oint_{S^-} S_{ijk}^*(\boldsymbol{\xi}^-, \mathbf{x}) \Delta u_k(\mathbf{x}) dS . \tag{9}$$

Hence, with using $\Sigma t_j(\boldsymbol{\xi}) = 0$, the traction equation can be written as

$$t_i(\boldsymbol{\xi}^-) = -n_j(\boldsymbol{\xi}^-)\oint_{S^-} S_{ijk}^*(\boldsymbol{\xi}^-, \mathbf{x}) \Delta u_k(\mathbf{x}) dS . \tag{10}$$

If the traction boundary conditions are given on the crack surface, we have

$$-n_j(\boldsymbol{\xi}^-)\oint_{S^-} S_{ijk}^*(\boldsymbol{\xi}^-, \mathbf{x}) \psi_k(\mathbf{x}) dS = t_i^0(\boldsymbol{\xi}^-) , \tag{11}$$

where $t_i^0(\boldsymbol{\xi}^-)$ is the specified traction on crack surface and displacement discontinuity $\psi_i(\mathbf{x}^-) = \Delta u_i(\mathbf{x}^-)$. By solving the above integral equation, the displacement discontinuities $\psi_i(\mathbf{x}^-)$ can be obtained. In the following analysis, we replace $\boldsymbol{\xi}^-$ and $\mathbf{x}^-$ with $\boldsymbol{\xi}$ and $\mathbf{x}$ for the sake of convenience of analysis.

2.3. *Relationship between T_{11} and T_{22} for mode I of plane crack*

Suppose a crack S is located on the plane $x_3 = 0$. Since $n_i = \delta_{i3}$, $\partial r / \partial n = r_{,3} = 0$ on S^-, the traction boundary integral equation Eq. (11) is simplified as

$$\oint\!\!\!\!\!\!-_{S^-} S_{ik}^*(\boldsymbol{\xi}, \mathbf{x})\psi_k(\mathbf{x})dS = -t_i^0(\boldsymbol{\xi}), \tag{12}$$

where $S_{ik}^*(\boldsymbol{\xi}, \mathbf{x}) := S_{i3k}^*(\boldsymbol{\xi}, \mathbf{x}) = \dfrac{E}{8\pi(1-\nu^2)r^3}\left\{3\nu r_{,i}r_{,k} + (1-2\nu)\delta_{ik} + 2\nu\delta_{k3}\delta_{i3}\right\}$ or

$$\begin{aligned}
S_{11}^* &= \frac{E}{8\pi(1-\nu^2)r^3}\left(1-\nu\frac{2(x_2-\xi_2)^2-(x_1-\xi_1)^2}{r^2}\right),\\
S_{12}^* &= S_{21}^* = \frac{E}{8\pi(1-\nu^2)r^3}\left(\frac{3\nu(x_1-\xi_1)(x_2-\xi_2)}{r^2}\right),\\
S_{22}^* &= \frac{E}{8\pi(1-\nu^2)r^3}\left(1-\nu\frac{2(x_1-\xi_1)^2-(x_2-\xi_2)^2}{r^2}\right),\\
S_{33}^* &= \frac{E}{8\pi(1-\nu^2)r^3},\quad S_{13}^* = S_{31}^* = S_{23}^* = S_{32}^* = 0,
\end{aligned} \tag{13}$$

with $r(\boldsymbol{\xi}, \mathbf{x}) = |\mathbf{x} - \boldsymbol{\xi}|$. For mode I fracture problem, we have $\psi_k(\mathbf{x}) = \psi_3(\mathbf{x})\delta_{k3}$. Then, from (13), $S_{i3}^*(\boldsymbol{\xi}, \mathbf{x}) = S_{33}^*(\boldsymbol{\xi}, \mathbf{x})\delta_{i3}$ and Eq. (12) becomes

$$\frac{E}{8\pi(1-\nu^2)}\oint\!\!\!\!\!\!-_{S^-}\frac{\psi_3(\mathbf{x})}{r(\boldsymbol{\xi}, \mathbf{x})^3}dS = -\sigma_3^0(\boldsymbol{\xi}), \tag{14a}$$

where $t_i^0(\boldsymbol{\xi}) = \sigma_3^0(\boldsymbol{\xi})\delta_{i3}$ is pressure load on the crack surface. In view of Eq. (11), the stresses on the crack surface under mode I are given as

$$\sigma_{ij}(\boldsymbol{\xi}) = -\oint\!\!\!\!\!\!-_{S^-} S_{ij3}^*(\boldsymbol{\xi}, \mathbf{x})\psi_3(\mathbf{x})dS \text{ with } S_{ij3}^*(\boldsymbol{\xi}, \mathbf{x}) = \frac{E}{8\pi(1-\nu^2)r^3}\left\{(1-2\nu)(3r_{,i}r_{,j} + 2\delta_{j3}\delta_{i3}) - (1-4\nu)\delta_{ij}\right\}. \tag{14b}$$

Thus,

$$\sigma_{11}(\boldsymbol{\xi}) = \frac{E}{8\pi(1-\nu^2)} \oint\limits_{S^-} \frac{1}{r^3}\left[(1-2\nu)\frac{3(x_1-\xi_1)^2}{r^2} - (1-4\nu)\right]\psi_3(\mathbf{x})dS,$$
$$\sigma_{22}(\boldsymbol{\xi}) = \frac{E}{8\pi(1-\nu^2)} \oint\limits_{S^-} \frac{1}{r^3}\left[(1-2\nu)\frac{3(x_2-\xi_2)^2}{r^2} - (1-4\nu)\right]\psi_3(\mathbf{x})dS, \tag{15}$$
$$\sigma_{12}(\boldsymbol{\xi}) = \frac{E}{8\pi(1-\nu^2)} \oint\limits_{S^-} \frac{1}{r^3}\left[(1-2\nu)\frac{3(x_1-\xi_1)(x_2-\xi_2)}{r^2}\right]\psi_3(\mathbf{x})dS.$$

Hence, and from Eq. (14)

$$\sigma_{11}(\mathbf{x}) + \sigma_{22}(\mathbf{x}) = \frac{(1+2\nu)E}{8\pi(1-\nu^2)} \oint\limits_{S^-} \frac{\psi_3(\mathbf{x})}{r^3} dS = -(1+2\nu)\sigma_3^0(\mathbf{x}). \tag{16}$$

According to the spatial distribution of stresses (1), one can find the following relationship for T-stresses

$$T_{11} + T_{22} = -(1+2\nu)\sigma_3^0, \tag{17}$$

where σ_3^0 is the applied constant pressure load on the crack surface.

It means that if one of the *T*-stresses is obtained, the other one can be determined consequently. Particularly, if the crack problems exhibit the symmetry with respect to the lines as shown in Figure 1, we know *T*-stresses immediately

$$T_{11} = T_{22} = -\frac{(1+2\nu)}{2}\sigma_3^0 \tag{18}$$

on the dash line.

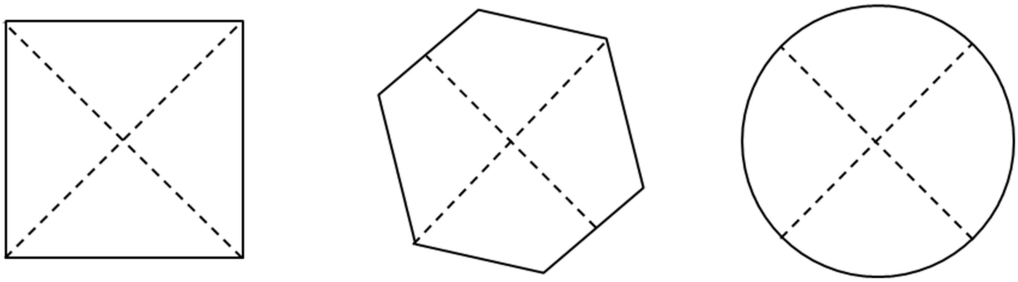

Figure 1. 2D crack area with symmetric axes.

3. Integral formulation for a rectangular crack in infinite domain

Consider a rectangular crack shown in Figure 2. In order to exclude more complicated singular behaviour at crack corners than that given by Eq. (1) and valid near a smooth crack front, a

rectangular crack with blunt corners is considered (a very small radius at corners of a rectangular is assumed). Because of the singularity of the stress near the crack front $x_1 = \pm a$ and $x_3 = \pm b$, the displacement discontinuity on the crack surface can be approximated as

$$\psi_k(\mathbf{x}) = \sum_{m=0}^{M}\sum_{n=0}^{N} c_k^{mn}\sqrt{1-(x_1/a)^2}U_m(x_1/a)\sqrt{1-(x_2/b)^2}U_n(x_2/b), \tag{19}$$

where c_k^{mn} represents the coefficient for different fracture modes, $U_m(x_1/a)$ and $U_n(x_2/b)$ are Chebyshev polynomials of the second kind which are defined as

$$U_n(x) = \frac{\sin[(n+1)\arccos(x)]}{\sin[\arccos(x)]}. \tag{20}$$

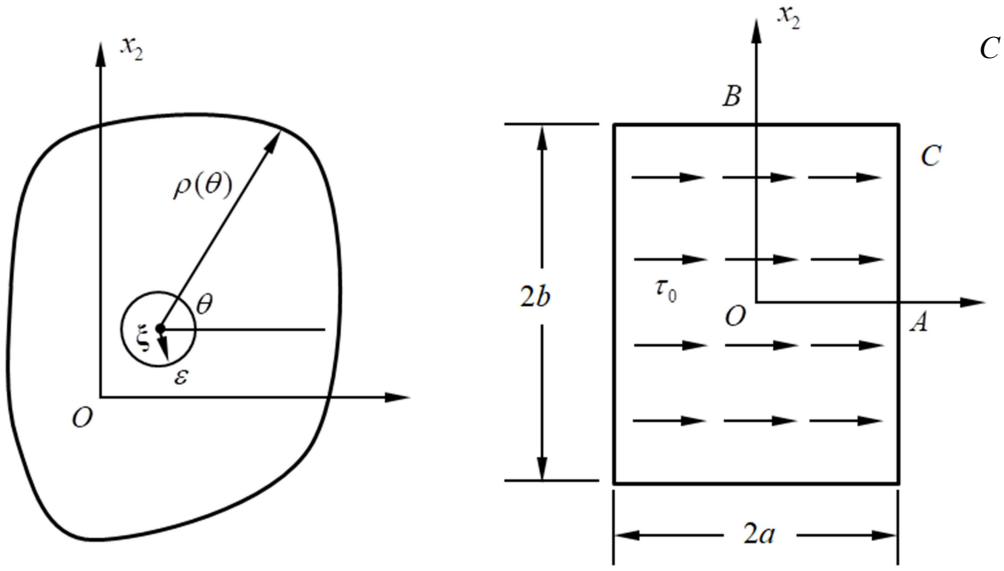

(a)

(b)

Figure 2. In plane crack in an infinite domain: (a) local integral coordinate; (b) rectangular crack under a shear distributed load.

Therefore, Eq. (14), for the mode I, becomes

$$\frac{E}{8\pi(1-\nu^2)}\sum_{m=0}^{M}\sum_{n=0}^{N} c_3^{mn}\int_{S^-}\frac{\sqrt{1-(x_1/a)^2}U_m(x_1/a)\sqrt{1-(x_2/b)^2}U_n(x_2/b)}{\sqrt{[(x_1-\xi_1)^2+(x_2-\xi_2)^2]^3}}dx_1dx_2 = -\sigma_3^0(\boldsymbol{\xi}), \tag{21}$$

where $\boldsymbol{\xi}=(\xi_1,\xi_2)$ indicates the collocation point on the crack surface. Introducing a polar coordinate system centered at location point (ξ_1,ξ_2) shown in Figure 2(a), the integral function $G_{mn}(\mathbf{x})=\sqrt{1-(x_1/a)^2}U_m(x_1/a)\sqrt{1-(x_2/b)^2}U_n(x_2/b)$ in Eq. (21) can be expanded around $\mathbf{x}=\boldsymbol{\xi}$ into Taylor series. Then,

$$\begin{aligned}\frac{G_{mn}(\mathbf{x})}{\rho^3}&=\frac{1}{\rho^3}\left\{G_{mn}(\mathbf{x})-\left[G_{mn}(\boldsymbol{\xi})+(x_1-\xi_1)G_{mn,1}(\boldsymbol{\xi})+(x_2-\xi_2)G_{mn,2}(\boldsymbol{\xi})\right]\right\}+\\&+\frac{1}{\rho^3}\left[G_{mn}(\boldsymbol{\xi})+(x_1-\xi_1)G_{mn,1}(\boldsymbol{\xi})+(x_2-\xi_2)G_{mn,2}(\boldsymbol{\xi})\right]+O(1/\rho),\end{aligned}\tag{22}$$

where $\rho=\sqrt{(x_1-\xi_1)^2+(x_2-\xi_2)^2}$, $x_1=\xi_1+\rho\cos\theta$, $x_2=\xi_2+\rho\sin\theta$, and

$$G_{mn,1}(\boldsymbol{\xi})=-\frac{(m+1)}{2\sqrt{1-(\xi_1/a)^2}}\left[U_{m+1}(\xi_1/a)-U_{m-1}(\xi_1/a)\right]\sqrt{1-(\xi_2/b)^2}U_n(\xi_2/b),\quad m\ge 1,$$

(23a)

$$G_{mn,2}(\boldsymbol{\xi})=-\frac{(n+1)}{2\sqrt{1-(\xi_2/b)^2}}\left[U_{n+1}(\xi_2/b)-U_{n-1}(\xi_2/b)\right]\sqrt{1-(\xi_1/a)^2}U_m(\xi_1/a),\quad n\ge 1,\tag{23b}$$

$$G_{0n,1}(\boldsymbol{\xi})=-\frac{\xi_1}{a\sqrt{1-(\xi_1/a)^2}}\sqrt{1-(\xi_2/b)^2}U_n(\xi_2/b),\tag{23c}$$

$$G_{m0,2}(\boldsymbol{\xi})=-\frac{\xi_2}{b\sqrt{1-(\xi_2/b)^2}}\sqrt{1-(\xi_1/a)^2}U_m(\xi_1/a).\tag{23d}$$

Therefore, using the local polar coordinate, the finite part integral in Eq. (21) becomes

$$\begin{aligned}A_{mn}(\boldsymbol{\xi})&=\oint\!\!\!\!\!\!-_{S^-}\frac{\sqrt{1-(x_1/a)^2}U_m(x_1/a)\sqrt{1-(x_2/b)^2}U_n(x_2/b)}{\sqrt{[(x_1-\xi_1)^2+(x_2-\xi_2)^2]^3}}\rho d\rho d\theta\\&=\int_0^{2\pi}\left\{\int_0^{\rho(\theta)}F_{mn}(\boldsymbol{\xi},\rho,\theta)d\rho-\frac{1}{\rho(\theta)}G_{mn}(\boldsymbol{\xi})+[G_{mn,1}(\boldsymbol{\xi})\cos\theta+G_{mn,2}(\boldsymbol{\xi})\sin\theta]\ln\rho(\theta)\right\}d\theta,\end{aligned}\tag{24}$$

where $\rho(\theta)$ is the distance between collocation point and the crack front as shown in Figure 2(a), and

$$F_{mn}(\boldsymbol{\xi},\rho,\theta)=\frac{1}{\rho^2}\left\{G_{mn}(\mathbf{x})-\left[G_{mn}(\boldsymbol{\xi})+\rho\cos\theta G_{mn,1}(\boldsymbol{\xi})+\rho\sin\theta G_{mn,2}(\boldsymbol{\xi})\right]\right\}\sim O(\rho^0).\tag{25}$$

Now, the integral A_{mn} can be calculated by any numerical integral scheme. There are two options for collocation point distribution $\boldsymbol{\xi}^{(pq)} = (\xi_1^{(pq)}, \xi_2^{(pq)})$, i.e.

(1) Chebyshev roots

$$\xi_1^{(pq)}/a = \cos\left(\frac{(2p+1)}{2(M+1)}\pi\right), \quad \xi_2^{(pq)}/b = \cos\left(\frac{(2q+1)}{2(N+1)}\pi\right), \quad p = 0,1,2,...,M, q = 0,1,2,...,N, \quad (26)$$

(2) Uniform distribution

$$\xi_1^{(pq)}/a = 1 - \frac{(2p+1)}{(M+1)}, \quad \xi_2^{(pq)}/b = 1 - \frac{(2q+1)}{(N+1)}, \quad p = 0,1,2,...,M, q = 0,1,2,...,N. \quad (27)$$

Then Eq. (21) at collocation point $\boldsymbol{\xi}^{(pq)}$ becomes

$$\frac{E}{8\pi(1-\nu^2)}\sum_{m=0}^{M}\sum_{n=0}^{N} A_{mn}(\boldsymbol{\xi}^{(pq)})c_3^{mn} = -\sigma_3^0(\boldsymbol{\xi}^{(pq)}) \qquad p = 0,1,2,...,M, q = 0,1,2,...,N. \quad (28)$$

Eq. (28) above provides a set of linear system of equation with $(M+1)(N+1)$ unknowns c_3^{mn}. Having known these coefficients, in view of Eq. (19), we can find the asymptotic behavior of displacement discontinuities near the crack front as

$$\begin{aligned}\lim_{r\to 0}\psi_3(x_1,x_2)\big|_{x_1=\pm(a-r)} &= \lim_{r\to 0}\sum_{m=0}^{M}\sum_{n=0}^{N} c_3^{mn}\sqrt{1-\left(\pm(a-r)/a\right)^2}U_m(\pm(a-r)/a)\sqrt{1-(x_2/b)^2}U_n(x_2/b)\\ &= \lim_{r\to 0}\sqrt{2r/a}\sum_{m=0}^{M}\sum_{n=0}^{N} c_3^{mn}U_m(\pm 1)\sqrt{1-(x_2/b)^2}U_n(x_2/b),\end{aligned} \quad (29a)$$

$$\begin{aligned}\lim_{r\to 0}\psi_3(x_1,x_2)\big|_{x_2=\pm(b-r)} &= \lim_{r\to 0}\sum_{m=0}^{M}\sum_{n=0}^{N} c_3^{mn}\sqrt{1-(x_1/a)^2}U_m(x_1/a)\sqrt{1-\left(\pm(b-r)/b\right)^2}U_n(\pm(b-r)/b)\\ &= \lim_{r\to 0}\sqrt{2r/b}\sum_{m=0}^{M}\sum_{n=0}^{N} c_3^{mn}\sqrt{1-(x_1/a)^2}U_m(x_1/a)U_n(\pm 1).\end{aligned}$$

On the other hand, from Eq. (2), we have

$$\lim_{r\to 0}\Delta u_3(r) = \lim_{r\to 0}\left[u_3(r,\theta)\big|_{\theta=\pi} - u_3(r,\theta)\big|_{\theta=-\pi}\right] = 4K_I\frac{1-\nu^2}{E}\lim_{r\to 0}\sqrt{\frac{2r}{\pi}}. \quad (29b)$$

Hence, we calculate the stress intensity factors along the crack front by

$$K_I(\pm a, x_2) = \frac{E}{4(1-\nu^2)a}\sum_{m=0}^{M}\sum_{n=0}^{N} c_3^{mn}U_m(\pm 1)\sqrt{1-(x_2/b)^2}U_n(x_2/b)\sqrt{\pi a}, \quad (30a)$$

$$K_I(x_1,\pm b) = \frac{E}{4(1-\nu^2)b}\sum_{m=0}^{M}\sum_{n=0}^{N} c_3^{mn}U_n(\pm 1)\sqrt{1-(x_1/a)^2}U_m(x_1/a)\sqrt{\pi b}, \quad (30b)$$

with $U_l(+1) = l+1$ and $U_l(-1) = (-1)^l(l+1)$ being known from the properties of the Chebyshev

polynomials. It is worth to mention that the Chebyshev polynomials of the first kind can be used in the boundary integral equation computation and the computational effort should be the same.

To evaluate the stresses at the collocation point $\xi^{(pq)}$ on the crack surface, Eq. (15) gives the following expression

$$\sigma_{ij}(\xi^{(pq)}) = \frac{E}{8\pi(1-\nu^2)} \sum_{m=0}^{M} \sum_{n=0}^{N} B_{mnij}(\xi^{(pq)}) c_3^{mn}, \tag{31}$$

where the coefficient is defined as

$$B_{mnij}(\xi^{(pq)}) = \int_0^{2\pi} \left(\int_0^{\rho(\theta)} F_{mn}(\xi^{(pq)}, \rho, \theta) d\rho - \frac{1}{\rho} G_{mn}(\xi^{(pq)}) + \Big[G_{mn,1}(\xi^{(pq)}) \cos\theta + G_{mn,2}(\xi^{(pq)}) \sin\theta \Big] \ln \rho(\theta) \right) g_{ij}(\theta) d\theta, \tag{32}$$

in which

$$g_{ij}(\theta) = (1-2\nu)(3\tau_i\tau_j + 2\delta_{j3}\delta_{i3}) - (1-4\nu)\delta_{ij}, \quad \tau_i = \delta_{i1}\cos\theta + \delta_{i2}\sin\theta \tag{33}$$

and $\int_0^{2\pi} [G_{mn,1}(\xi)\cos\theta + G_{mn,2}(\xi)\sin\theta] d\theta = 0$ is observed. Same procedure above can be applied to calculate the stress intensity factors and *T*-stresses for mixed mode fracture problems.

It is worth to notice that in general mixed mode fracture problems, the boundary integral equations (12) can be written, at collocation point $\xi^{(pq)}$, as

$$\frac{E}{8\pi(1-\nu^2)} \sum_{m=0}^{M} \sum_{n=0}^{N} A_{mn}(\xi^{(pq)}) c_k^{mn} = -t_k^0(\xi^{(pq)}) \qquad p = 0,1,2,...,M, q = 0,1,2,...,N, k = 1,2,3, \tag{34}$$

where $t_k^0(\xi)$ presents the traction specified on the crack surface. For the mixed mode stress intensity factors along the crack front, we have

$$K_{\mathrm{II}}(\pm a, x_2) = \frac{E}{4(1-\nu^2)a} \sum_{m=0}^{M} \sum_{n=0}^{N} c_1^{mn} U_m(\pm 1) \sqrt{1-(x_2/b)^2}\, U_n(x_2/b) \sqrt{\pi a}\ , \tag{35a}$$

$$K_{\mathrm{II}}(x_1, \pm b) = \frac{E}{4(1-\nu^2)b} \sum_{m=0}^{M} \sum_{n=0}^{N} c_1^{mn} U_n(\pm 1) \sqrt{1-(x_1/a)^2}\, U_m(x_1/a) \sqrt{\pi b}, \tag{35b}$$

$$K_{\mathrm{III}}(\pm a, x_2) = \frac{E}{4(1+\nu)a} \sum_{m=0}^{M} \sum_{n=0}^{N} c_2^{mn} U_m(\pm 1) \sqrt{1-(x_2/b)^2}\, U_n(x_2/b) \sqrt{\pi a}\ , \tag{35c}$$

$$K_{\mathrm{III}}(x_1, \pm b) = \frac{E}{4(1+\nu)b} \sum_{m=0}^{M} \sum_{n=0}^{N} c_2^{mn} U_n(\pm 1) \sqrt{1-(x_1/a)^2}\, U_m(x_1/a) \sqrt{\pi b}\ , \tag{35d}$$

because the displacement discontinuities in the II and III mode are given, respectively, according

to Eq. (2) by

$$\lim_{r\to 0}\Delta u_1(r)=\lim_{r\to 0}\left[u_1(r,\theta)\big|_{\theta=\pi}-u_1(r,\theta)\big|_{\theta=-\pi}\right]=4K_{\mathrm{II}}\frac{1-\nu^2}{E}\lim_{r\to 0}\sqrt{\frac{2r}{\pi}}\ , \tag{35e}$$

$$\lim_{r\to 0}\Delta u_2(r)=\lim_{r\to 0}\left[u_2(r,\theta)\big|_{\theta=\pi}-u_2(r,\theta)\big|_{\theta=-\pi}\right]=4K_{\mathrm{III}}\frac{1+\nu}{E}\lim_{r\to 0}\sqrt{\frac{2r}{\pi}}\ . \tag{35f}$$

Let us consider a rectangular crack in infinite domain is subjected to a uniformly distributed pressure load σ_0 on the surface which is equivalent to that under a remote tensile load. The maximum numbers of the Chebyshev polynomials M and N are selected as 10. Poisson's ratio $\nu=0.3$ and Young's modulus is one unit. The numerical solution of the normalized stress intensity factors, $K_{\mathrm{I}}(a,x_2)/\sigma_0\sqrt{\pi a}$ and $K_{\mathrm{I}}(x_1,b)/\sigma_0\sqrt{\pi a}$, along the crack fronts AC and BC, are given in Figures 3 and 4 respectively. The normalised normal *T*-stress $T_{11}(a,x_2)/\sigma_0$ and shear *T*-stress $T_{12}(a,x_2)/\sigma_0$ are presented in Figures 5 and 6. It can be seen from Figures 5 and 6, the maximum *T*-stress $T_{11}(a,x_2)$ is at the center of the edge and $T_{12}(a,x_2)$ is monotone function from the center (zero) to the corner of the crack. For large ratio of b/a, $T_{11}(a,x_2)/\sigma_0$ at the center tends to -1 as we expected. In order to observe the convergence of the computational method, the normalized stress intensity factors $K_I/\sigma_0\sqrt{\pi a}$ at point A versus the numbers M and N for different node distributions are shown in Table 1, while $b/a=1$. Comparison of the maximum stress intensity factor at pint A between the numerical solution and analytical results from the handbook [40] are shown in Figure 7. We observe excellent agreement between those solutions for both two node distributions even with a few nodes such as 9 nodes in total (3×3). Secondly, we consider a rectangular crack in infinite body subjected to uniform distributed shear load τ_0 on the surface shown in Figure 2(b). The normalized stress intensity factors $K_{\mathrm{II}}(b/a)/\tau_0\sqrt{\pi a}$ at crack tip $A(a,0)$ and $K_{\mathrm{III}}(b/a)/\tau_0\sqrt{\pi a}$ at tip $B(0,b)$ are plotted in Figure 8 with different Poisson's ratios. In this case, all *T*-stresses are zeros along the crack front. The influence of Poisson's ratio on the shearing and tearing stress intensity factors is observable.

Table 1. Normalized SIF with node numbers

$M = N$	Chebyshev	Uniform
2	0.7604	0.7567
4	0.7529	0.7539
6	0.7551	0.7535
8	0.7574	0.7535
10	0.7556	0.7535

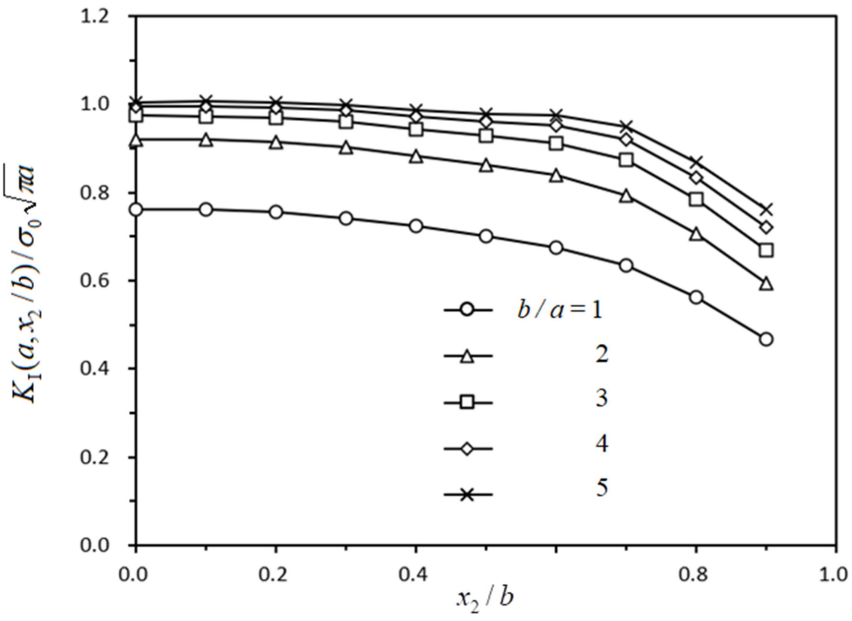

Figure 3. Normalized stress intensity factor along the crack front AC under uniform pressure load.

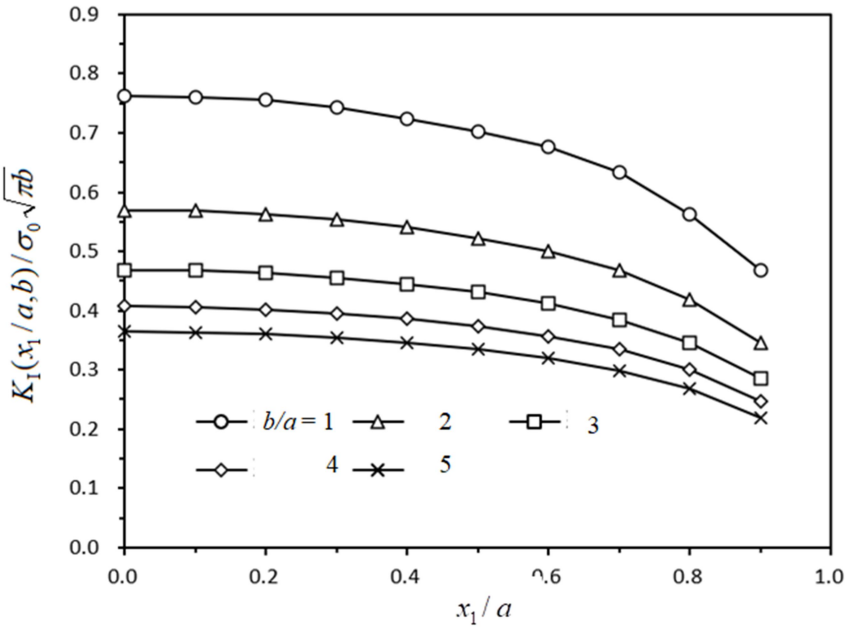

Figure 4. Normalized stress intensity factor along the crack front BC under uniform pressure load.

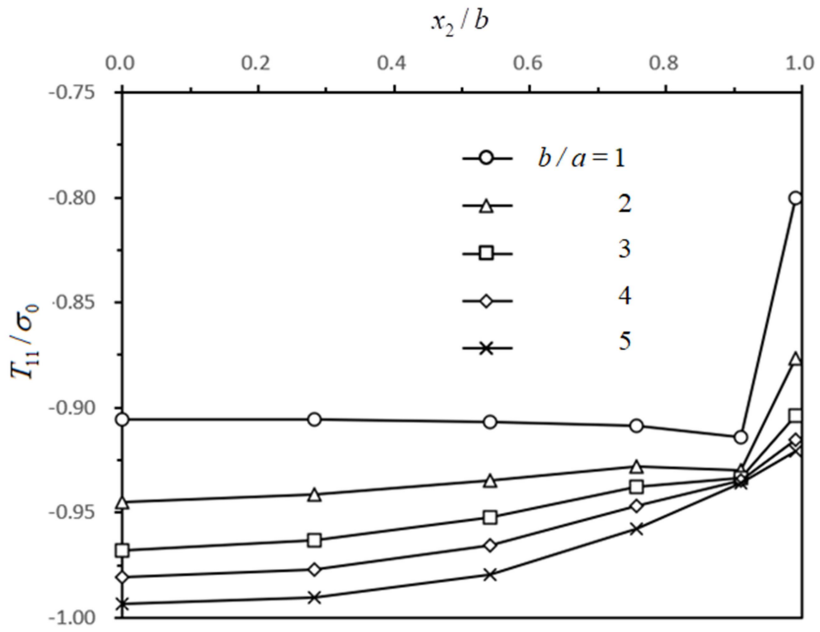

Figure 5. Normalized *T*-stress T_{11}/σ_0 along the crack front AC.

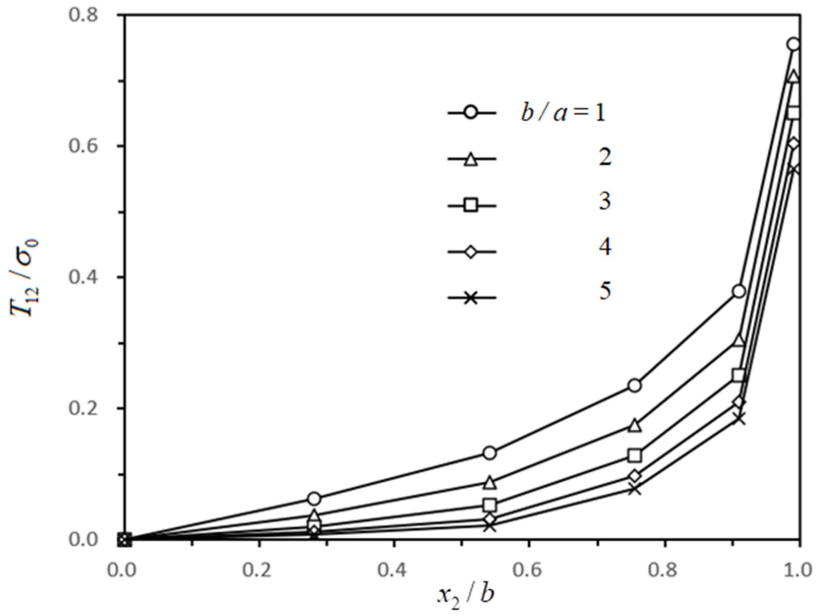

Figure 6. Normalized *T*-stress T_{12}/σ_0 along the crack front AC.

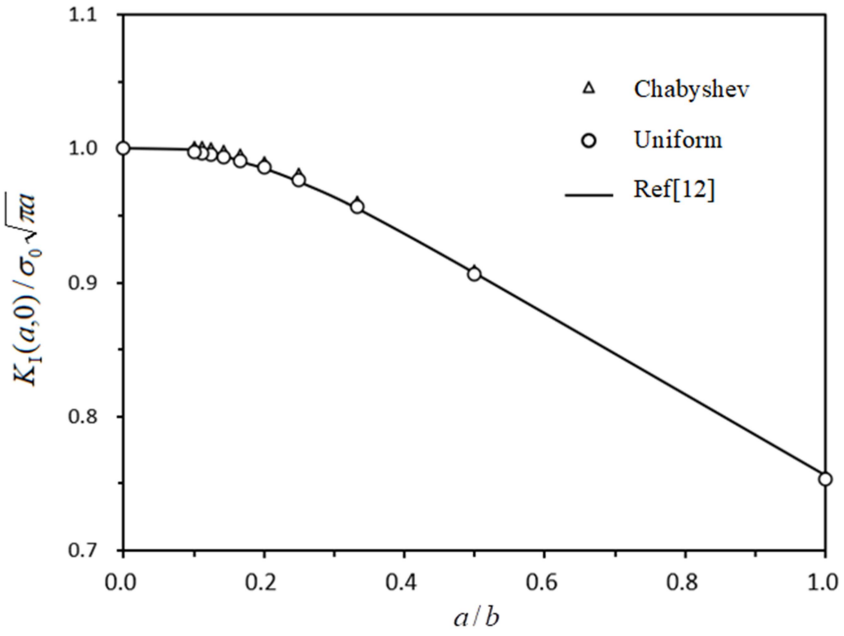

Figure 7. Normalized stress intensity factor $K_I/\sigma_0\sqrt{\pi a}$ at point A under pressure load.

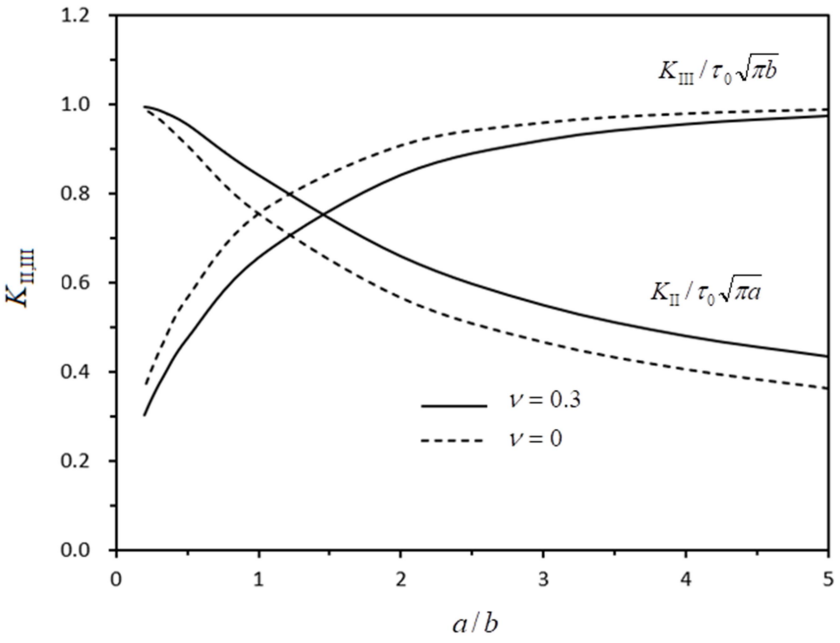

Figure 8. Normalized stress intensity factors $K_{\mathrm{II}}/\tau_0\sqrt{\pi a}$ at point A and $K_{\mathrm{III}}/\tau_0\sqrt{\pi b}$ at point B under uniform distributed shear load.

4. Integral formulation for an elliptical crack

Consider an elliptical crack shown in Figure 9. The Cartesian coordinates of the point $\mathbf{x}$ on the crack surface can be expressed in terms of two parametric coordinates (t,φ) as

$$x_1 = at\cos\varphi\,,\ x_2 = bt\sin\varphi \ \text{ with } t\in[0,1],\ \ \varphi\in[0,2\pi]\,, \tag{36a}$$

where a and b indicate the lengths of the semi-major and semi-minor axes. Then, the t-coordinate of the crack front points $C(1,\varphi)$ is fixed $t=1$. The Cartesian coordinates of the collocation point $\boldsymbol{\xi}^{(pq)}$ on the crack surface can be expressed as

$$\xi_1^{(pq)} = at^{(p)}\cos\varphi^{(q)},\ \xi_2^{(pq)} = bt^{(p)}\sin\varphi^{(q)},\ t^{(p)}\le 1,\ 0\le\varphi^{(q)}\le 2\pi\,. \tag{36b}$$

Besides the coordinates (t,φ), it is appropriate to introduce also the polar coordinates (ρ,θ) centered at (ξ_1,ξ_2). Then,

$$x_1 = \xi_1+\rho\cos\theta = at\cos\varphi\,,\ \ x_2 = \xi_2+\rho\sin\theta = bt\sin\varphi\,,\ \rho=\sqrt{(x_1-\xi_1)^2+(x_2-\xi_2)^2}\,. \tag{37a}$$

Hence,

$$t=\left[\left(\xi_1+\rho\cos\theta\right)^2/a^2+\left(\xi_2+\rho\sin\theta\right)^2/b^2\right]^{1/2},\varphi=\arctan\left(\frac{a}{b}\frac{\xi_2+\rho\sin\theta}{\xi_1+\rho\cos\theta}\right)\text{ and }dx_1dx_2=\rho d\rho d\theta. \quad (37b)$$

Similar to a rectangular crack, the displacement discontinuity of the crack can be approximated as

$$\psi_k(x_1,x_2)=\sum_{m=0}^{M}\sum_{n=0}^{N}c_k^{mn}\sqrt{1-t^2}U_m(t)U_n(\overline{\varphi}),\ \ t\le 1,\ 0\le\overline{\varphi}\le 1, \quad (38)$$

where $\overline{\varphi}=\varphi/2\pi$ and c_k^{mn} represents the coefficient for different fracture modes. Therefore, the boundary integral equation in Eq. (14) for mode I problem becomes

$$\frac{E}{8\pi(1-\nu^2)}\sum_{m=0}^{M}\sum_{n=0}^{N}c_3^{mn}\int_{S^-}\frac{\sqrt{1-t^2}U_m(t)U_n(\overline{\varphi})}{\sqrt{[(x_1-\xi_1)^2+(x_2-\xi_2)^2]^3}}dx_1dx_2=-\sigma_3^0(\boldsymbol{\xi}). \quad (39)$$

In order to perform the integration in finite part sense, we need to extract specific singular terms in the integrand with singularity ρ^{-3}. This can be done by expanding the function $G_{mn}(t,\overline{\varphi})=\sqrt{1-t^2}U_m(t)U_n(\overline{\varphi})$ into Taylor series with respect to ρ around $\rho=0$ as

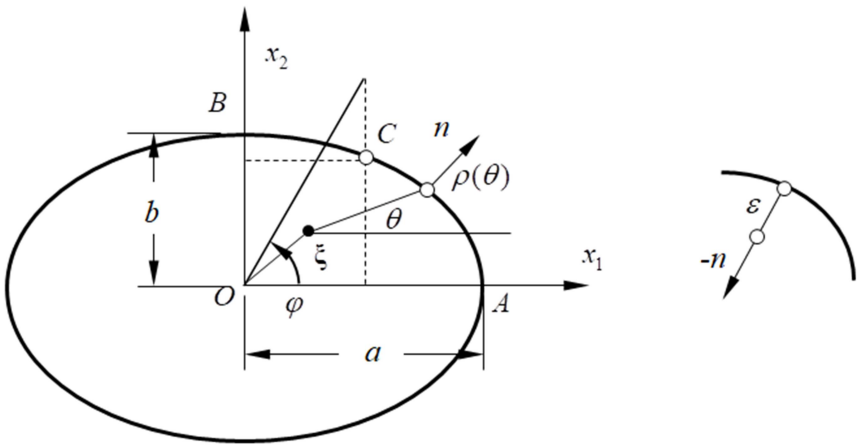

(a) (b)

Figure 9. Elliptical crack: (a) coordinate of collocation point; (b) collocation point near the boundary with small gap ε along normal direction.

$$G_{mn}(t,\overline{\varphi})=G_{mn}^{(0)}(\boldsymbol{\xi})+\rho\left(\left.\frac{\partial t}{\partial\rho}\right|_{\rho=0}G_{mn}^{(1)}(\boldsymbol{\xi})+\left.\frac{\partial\overline{\varphi}}{\partial\rho}\right|_{\rho=0}G_{mn}^{(2)}(\boldsymbol{\xi})\right)+O\left(\rho^2\right) \quad (40)$$

with

$$G_{mn}^{(0)}(\boldsymbol{\xi})=G_{mn}(t,\overline{\varphi})\big|_{\rho=0}, \quad (41a)$$

$$G_{mn}^{(1)}(\boldsymbol{\xi})=\left.\frac{\partial G_{mn}(t,\bar{\varphi})}{\partial t}\right|_{\rho=0}=-\left.\frac{(m+1)}{2\sqrt{1-t^2}}\left[U_{m+1}(t)-U_{m-1}(t)\right]U_n(\bar{\varphi})\right|_{\rho=0},\quad m\ge 1 \tag{41b}$$

$$G_{0n}^{(1)}(\boldsymbol{\xi})==\left.\frac{\partial G_{0n}(t,\bar{\varphi})}{\partial t}\right|_{\rho=0}=-\left.\frac{t}{\sqrt{1-t^2}}U_n(\bar{\varphi})\right|_{\rho=0},$$

(41c)

$$G_{mn}^{(2)}(\boldsymbol{\xi})=\left.\frac{\partial G_{mn}(t,\bar{\varphi})}{\partial \bar{\varphi}}\right|_{\rho=0}=\left.\frac{1}{1-\bar{\varphi}^2}\left[(n+1)U_{n-1}(\bar{\varphi})-n\bar{\phi}U_n(\bar{\varphi})\right]\sqrt{1-t^2}U_m(t)\right|_{\rho=0},\quad n\ge 1 \tag{41d}$$

$$G_{m0}^{(2)}(\boldsymbol{\xi})=\left.\frac{\partial G_{m0}(t,\bar{\varphi})}{\partial \bar{\varphi}}\right|_{\rho=0}=\left.\frac{\partial}{\partial \bar{\varphi}}\sqrt{1-t^2}U_m(t)\right|_{\rho=0}=0, \tag{41e}$$

$$t\big|_{\rho=0}=\left(\left(\xi_1/a\right)^2+\left(\xi_2/b\right)^2\right)^{1/2},\qquad \bar{\varphi}\big|_{\rho=0}=\frac{1}{2\pi}\arctan\left(\frac{a}{b}\frac{\xi_2}{\xi_1}\right), \tag{41f}$$

$$\frac{\partial t}{\partial \rho}=\frac{1}{t}\left(\frac{\xi_1+\rho\cos\theta}{a}\frac{\cos\theta}{a}+\frac{\xi_2+\rho\sin\theta}{b}\frac{\sin\theta}{b}\right),\qquad \frac{\partial \varphi}{\partial \rho}=\frac{1}{ab}\frac{\xi_1\sin\theta-\xi_2\cos\theta}{t^2}, \tag{41g}$$

$$\left.\frac{\partial t}{\partial \rho}\right|_{\rho=0}=\left(\frac{\xi_1\cos\theta}{a^2}+\frac{\xi_2\sin\theta}{b^2}\right)\left[\left(\frac{\xi_1}{a}\right)^2+\left(\frac{\xi_2}{b}\right)^2\right]^{-1/2},\qquad \left.\frac{\partial \bar{\varphi}}{\partial \rho}\right|_{\rho=0}=\frac{1}{2\pi ab}\frac{\xi_1\sin\theta-\xi_2\cos\theta}{(\xi_1/a)^2+(\xi_2/b)^2}. \tag{41h}$$

Then,

$$\frac{\sqrt{1-t^2}U_m(t)U_n(\bar{\varphi})}{\sqrt{[(x_1-\xi_1)^2+(x_2-\xi_2)^2]^3}}=F_{mn}(\boldsymbol{\xi},\rho,\theta)+\frac{1}{\rho^3}G_{mn}^{(0)}(\boldsymbol{\xi})+\frac{1}{\rho^2}\left(\left.\frac{\partial t}{\partial \rho}\right|_{\rho=0}G_{mn}^{(1)}(\boldsymbol{\xi})+\left.\frac{\partial \bar{\varphi}}{\partial \rho}\right|_{\rho=0}G_{mn}^{(2)}(\boldsymbol{\xi})\right), \tag{42}$$

where

$$F_{mn}(\boldsymbol{\xi},\rho,\theta)=\frac{1}{\rho^3}\left\{G_{mn}(t,\bar{\varphi})-G_{mn}^{(0)}(\boldsymbol{\xi})-\rho\left(\left.\frac{\partial t}{\partial \rho}\right|_{\rho=0}G_{mn}^{(1)}(\boldsymbol{\xi})+\left.\frac{\partial \bar{\varphi}}{\partial \rho}\right|_{\rho=0}G_{mn}^{(2)}(\boldsymbol{\xi})\right)\right\}\sim O\left(\rho^{-1}\right). \tag{43}$$

Hence, the integral in Eq. (39) becomes

$$\begin{aligned}A_{mn}(\boldsymbol{\xi})&=\oint\limits_{S^-}\frac{\sqrt{1-t^2}U_m(t)U_n(\bar{\phi})}{\sqrt{[(x_1-\xi_1)^2+(x_2-\xi_2)^2]^3}}\rho d\rho d\theta\\&=\int\limits_0^{2\pi}\left[\int\limits_0^{\rho(\theta)}\rho F_{mn}(\boldsymbol{\xi},\rho,\theta)d\rho-\frac{1}{\rho(\theta)}G_{mn}^{(0)}(\boldsymbol{\xi})+\left(\left.\frac{\partial t}{\partial \rho}\right|_{\rho=0}G_{mn}^{(1)}(\boldsymbol{\xi})+\left.\frac{\partial \bar{\varphi}}{\partial \rho}\right|_{\rho=0}G_{mn}^{(2)}(\boldsymbol{\xi})\right)\ln\rho(\theta)\right]d\theta,\end{aligned} \tag{44}$$

where $\rho(\theta)$ is the maximal distance between the collocation point and integration points $\mathbf{x}(\rho,\theta)\in S^-$; it is shown in Fig. (9) and expressed in Appendix A. As the integral function above

is regular, the integral can be evaluated using Gaussian integration. Eq. (39) provides a set of linear system of equations with $(M+1)(N+1)$ unknowns c_3^{mn}. Two normalized parameter in Eq. (36) are uniformly distributed, as

$$t^{(p)} = 1 - \frac{(2p+1)}{(M+1)}, \quad \varphi^{(q)}/2\pi = 1 - \frac{(2q+1)}{(N+1)}, \quad p = 0,1,2,...,M, q = 0,1,2,...,N, \tag{45}$$

and then we have

$$\xi_1^{(pq)} = at^{(p)}\cos\varphi^{(q)}, \ \xi_2^{(pq)} = bt^{(p)}\sin\varphi^{(q)}. \tag{46}$$

In order to determine the stress intensity factors, we need to know

$$\lim_{\varepsilon\to 0}\frac{\Delta u_k(\mathbf{x}^\varepsilon)}{\sqrt{\varepsilon}} = \lim_{\varepsilon\to 0}\frac{\psi_k(\mathbf{x}^\varepsilon)}{\sqrt{\varepsilon}}, \tag{47}$$

where $\mathbf{x}^\varepsilon = \mathbf{x}^f - \varepsilon\mathbf{n}(\mathbf{x}^f)$, with $\left(x_1^\varepsilon, x_2^\varepsilon\right) = \left(at\cos\varphi, bt\sin\varphi\right)$, $t<1$ and $\left(x_1^f, x_2^f\right) = \left(a\cos\varphi, b\sin\varphi\right)$ being the interior point on the crack surface and the point the crack front, respectively, and the unit outward normal vector $\mathbf{n}(\mathbf{x}^f)$ to the crack front at $\mathbf{x}^f$ is given by (A7) in Appendix.

Since $\psi_k(\mathbf{x}^\varepsilon) = -\varepsilon\left.\frac{\partial\psi_k}{\partial\mathbf{n}}\right|_{t=1} + O(\varepsilon^2)$, we may write

$$\begin{aligned}
&\lim_{\varepsilon\to 0}\frac{\psi_k(\mathbf{x}^\varepsilon)}{\sqrt{\varepsilon}} = -\lim_{\varepsilon\to 0}\sqrt{\varepsilon}\left.\frac{\partial\psi_k}{\partial\mathbf{n}}\right|_{t=1} = -\lim_{\varepsilon\to 0}\sqrt{\varepsilon}\lim_{t\to 1}\left(\frac{\partial t}{\partial\mathbf{n}}\frac{\partial\psi_k}{\partial t}\right) = \\
&= -\left(\frac{\cos\varphi}{a}n_1 + \frac{\sin\varphi}{b}n_2\right)\lim_{\varepsilon\to 0}\sqrt{\varepsilon}\lim_{t\to 1}\left[\frac{\partial\sqrt{1-t^2}}{\partial t} + \sqrt{1-t^2}\,\frac{\partial}{\partial t}\right]\sum_{m=0}^{M}\sum_{n=0}^{N}c_k^{mn}U_m(t)U_n(\overline{\varphi}) = \\
&= \frac{\sqrt{(a\sin\varphi)^2 + (b\cos\varphi)^2}}{ab}\sum_{m=0}^{M}\sum_{n=0}^{N}c_k^{mn}U_m(1)U_n(\overline{\varphi})\lim_{\varepsilon\to 0}\sqrt{\frac{\varepsilon}{2(1-t)}},
\end{aligned} \tag{48a}$$

where we have utilized (38), (A7) and

$$\frac{\partial t}{\partial x_i^\varepsilon} = \frac{\cos\varphi}{a}\delta_{i1} + \frac{\sin\varphi}{b}\delta_{i2} = \frac{\partial t}{\partial x_i^f}, \text{ because } t = \sqrt{(x_1^\varepsilon/a)^2 + (x_2^\varepsilon/b)^2}. \tag{48b}$$

Furthermore,

$$\begin{aligned}
t &= \sqrt{\left(\frac{x_1^f - \varepsilon n_1}{a}\right)^2 + \left(\frac{x_2^f - \varepsilon n_2}{b}\right)^2} = \sqrt{\left(\frac{x_1^f}{a}\right)^2 + \left(\frac{x_2^f}{b}\right)^2 - 2\varepsilon\left(\frac{n_1 x_1^f}{a^2} + \frac{n_2 x_2^f}{b^2}\right) + \left(\frac{\varepsilon n_1}{a}\right)^2 + \left(\frac{\varepsilon n_2}{b}\right)^2} = \\
&= 1 - \varepsilon\left(\frac{n_1 x_1^f}{a^2} + \frac{n_2 x_2^f}{b^2}\right) + O(\varepsilon^2) = 1 - \frac{\varepsilon}{ab}\sqrt{(a\sin\varphi)^2 + (b\cos\varphi)^2} + O(\varepsilon^2),
\end{aligned} \tag{49a}$$

hence,

$$\lim_{\varepsilon\to 0}\sqrt{\frac{\varepsilon}{2(1-t)}}=\frac{\sqrt{ab/2}}{\left[(a\sin\varphi)^2+(b\cos\varphi)^2\right]^{1/4}}. \tag{49b}$$

In view of (48) and (49), we have

$$\lim_{\varepsilon\to 0}\frac{\psi_k(\mathbf{x}^{\varepsilon})}{\sqrt{\varepsilon}}=\frac{\left[(a\sin\varphi)^2+(b\cos\varphi)^2\right]^{1/4}}{\sqrt{2ab}}\sum_{m=0}^{M}\sum_{n=0}^{N}c_k^{mn}U_m(1)U_n(\overline{\varphi}). \tag{50}$$

Since $\lim_{\varepsilon\to 0}\frac{\Delta u_3(\mathbf{x}^{\varepsilon})}{\sqrt{\varepsilon}}=K_I\sqrt{\frac{2}{\pi}}\frac{4(1-\nu^2)}{E}$ according to Eq. (2), and bearing in mind (47), (50), the mode I stress intensity factor is

$$K_I=\frac{E\sqrt{\pi}}{8(1-\nu^2)}\frac{\left[(a\sin\varphi)^2+(b\cos\varphi)^2\right]^{1/4}}{\sqrt{ab}}\sum_{m=0}^{M}\sum_{n=0}^{N}c_3^{mn}U_m(1)U_n(\overline{\varphi}). \tag{51}$$

The analytical solution of the stress intensity factor for an elliptical crack in infinite body subjected to a uniform pressure load is [41]

$$K_1(1,\overline{\varphi})=\frac{\sigma_0\sqrt{\pi a}}{E(\kappa)}\Theta\ , \tag{52}$$

where $E(\kappa)$ denotes a complete elliptical integral of second kind,

$$E(\kappa)=\int_0^{\pi/2}\sqrt{1-\kappa^2\sin^2\varphi}\,d\varphi,\ \Theta=\left(\frac{a^2}{b^2}\sin^2\varphi+\cos^2\varphi\right)^{1/4},\ \kappa=\sqrt{1-\frac{b^2}{a^2}}. \tag{53}$$

5. Integral formulation for a rectangular crack on a cylinder surface

Consider a rectangular crack $(w\times h)$ on a cylinder surface of radius *R* subjected to a remote tensile load shown in Figure 10(a). The displacement discontinuity of the crack is approximated as

$$\psi_k(s_1,s_2)=\sum_{m=0}^{M}\sum_{n=0}^{N}c_k^{mn}\sqrt{1-(s_1/w)^2}U_m(s_1/w)\sqrt{1-(s_2/h)^2}U_n(s_2/h), \tag{54}$$

where s_1 and s_2 are natural coordinates on the crack surface, with $s_2\in[0,h]$, $s_1\in[0,w]$, $w=R\arcsin(a/R)$. The integral equation in Eq. (11) becomes

$$\sum_{m=0}^{M}\sum_{n=0}^{N}c_k^{mn}n_j(\xi)\oint_{S^-}\sqrt{1-(s_1/w)^2}U_m(s_1/w)\sqrt{1-(s_2/h)^2}U_n(s_2/h)S_{ijk}^{*}(\xi,\rho,\theta)ds_1ds_2=-t_i^0(\xi), \tag{55}$$

where $\boldsymbol{\xi}(\mathbf{s}')$ indicates the collocation point on crack surface

$$\xi_1 = R\sin\frac{s_1'}{R}, \quad \xi_2 = s_2', \quad \xi_3 = R\cos\frac{s_1'}{R}, \tag{56}$$

and $\mathbf{s} = (s_1, s_2)$ indicates the natural coordinates of the domain integral field point on the curved crack surface

$$x_1 = R\sin\left(\frac{s_1}{R}\right), \quad x_2 = s_2, \quad x_3 = R\cos\left(\frac{s_1}{R}\right). \tag{57}$$

The cylindrical crack surface is mapped into rectangular domain as shown in Figure 10(b) or into the non-dimensional rectangle as shown in Figure B1 in Appendix B. It is appropriate to introduce the local polar coordinate system centered at the collocation point $\mathbf{s}'$. Then, $ds_1 ds_2 = \rho d\rho d\theta = wh\, d\eta_1 d\eta_2 = wh\zeta d\zeta d\theta$ and the integrand in Eq. (57) can be rearranged by using the Taylor series expansion for extraction of relevant singular terms as given in Appendix B.

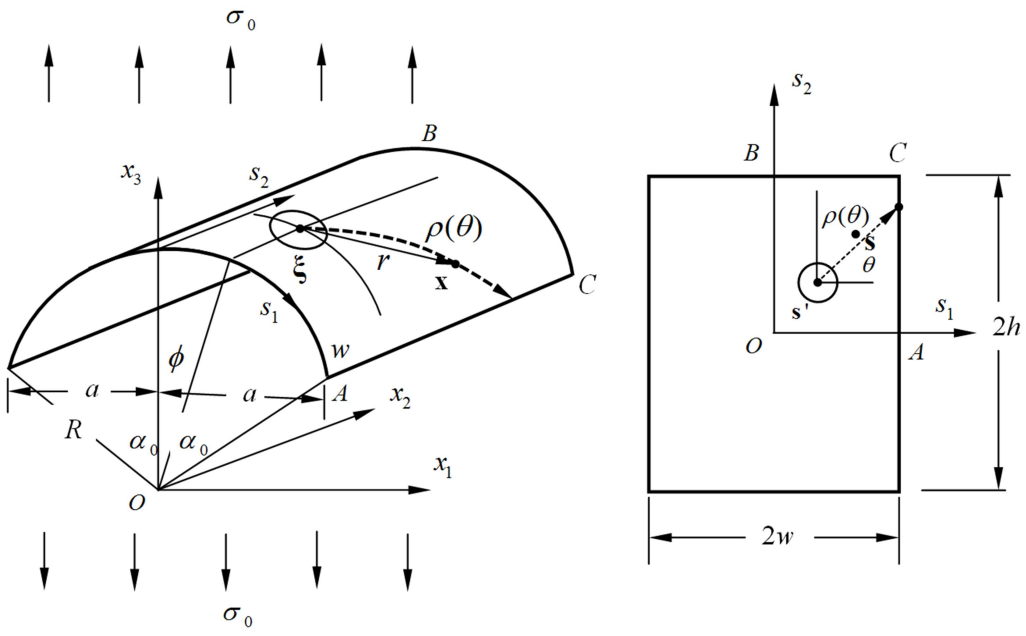

(a) (b)

Figure 10. A rectangular crack on a cylinder surface in an infinite domain subjected to a remote tensile force σ_0 .(a) 3D global coordinate (x_1, x_2, x_3) and nature coordinate for cylindrical surface crack; (b) local 2D coordinate of nature coordinate system $(s_1 o s_2)$.

In view of (B10) and (B15), the integral equation (57) considered at the collocation points $\boldsymbol{\xi}^{pq}=(\xi_1^{(p)},\xi_2^{(q)})=\left(R\sin(s_1'^{(p)}/R),s_2'^{(q)},R\cos(s_1'^{(p)}/R)\right)$ becomes

$$\sum_{m=0}^{M}\sum_{n=0}^{N}c_k^{mn}A_{mnik}(s_1'^{(p)},s_2'^{(q)})=-t_i^0(\boldsymbol{\xi}^{(pq)}),\ (p=0,1,...,M),(q=0,1,...,N),(i,k=1,2,3) \tag{58}$$

where $A_{mnik}(s_1',s_2')$ is given by Eq. (B15) in which all integrations can be performed by standard integration schemes because the integrands are nonsingular functions of the integration variables (ζ,θ). Equation (60) provides a linear system of equation with $3\times(M+1)(N+1)$ unknowns c_k^{mn}. With solving this linear algebraic equations, we find the stress intensity factors along the crack front. Recall that the asymptotic relationships (2) are related to the specific local coordinate system with the third axis along the normal vector $\mathbf{n}$, the first axis along $\boldsymbol{\tau}$ and the second axis along $\boldsymbol{\rho}$, where $n_i(\pm w,s_2)=\delta_{i1}\sin(\pm w/R)+\delta_{i3}\cos(\pm w/R)$, $\tau_i(\pm w,s_2)=n_3\delta_{i1}-n_1\delta_{i3}$, $\rho_i(\pm w,s_2)=\pm\delta_{i2}$ on the crack front AC, while $n_i(s_1,\pm h)=\delta_{i1}\sin(s_1/R)+\delta_{i3}\cos(s_1/R)$, $\tau_i(s_2,\pm h)=\pm\delta_{i2}$, $\rho_i(s_1,\pm h)=\mp n_3\delta_{i1}\pm n_1\delta_{i3}$ on the crack front BC. Thus, we have on the crack front AC:

$$\begin{aligned}n_k(\pm w,s_2)\lim_{\varepsilon\to0}\Delta u_k\left(\pm R\sin\frac{w-\varepsilon}{R},s_2,R\cos\frac{w-\varepsilon}{R}\right)&=4K_{\mathrm{I}}\frac{1-\nu^2}{E}\lim_{\varepsilon\to0}\sqrt{\frac{2\varepsilon}{\pi}}=n_k\lim_{\varepsilon\to0}\psi_k\left(\pm(w-\varepsilon),s_2\right)=\\&=\left(\delta_{k3}\cos\frac{w}{R}\pm\delta_{k1}\sin\frac{w}{R}\right)\sum_{m=0}^{M}\sum_{n=0}^{N}c_k^{mn}U_m(\pm1)\sqrt{1-(s_2/h)^2}U_n(s_2/h)\lim_{\varepsilon\to0}\sqrt{\frac{2\varepsilon}{w}}\end{aligned} \tag{59}$$

$$\begin{aligned}\tau_k(\pm w,s_2)\lim_{\varepsilon\to0}\Delta u_k\left(\pm R\sin\frac{w-\varepsilon}{R},s_2,R\cos\frac{w-\varepsilon}{R}\right)&=4K_{\mathrm{II}}\frac{1-\nu^2}{E}\lim_{\varepsilon\to0}\sqrt{\frac{2\varepsilon}{\pi}}=\tau_k\lim_{\varepsilon\to0}\psi_k\left(\pm(w-\varepsilon),s_2\right)=\\&=\left(\cos\frac{w}{R}\delta_{k1}\mp\sin\frac{w}{R}\delta_{k3}\right)\sum_{m=0}^{M}\sum_{n=0}^{N}c_k^{mn}U_m(\pm1)\sqrt{1-(s_2/h)^2}U_n(s_2/h)\lim_{\varepsilon\to0}\sqrt{\frac{2\varepsilon}{w}}\end{aligned} \tag{60}$$

$$\begin{aligned}\rho_k(\pm w,s_2)\lim_{\varepsilon\to0}\Delta u_k\left(\pm R\sin\frac{w-\varepsilon}{R},s_2,R\cos\frac{w-\varepsilon}{R}\right)&=4K_{\mathrm{III}}\frac{1+\nu}{E}\lim_{\varepsilon\to0}\sqrt{\frac{2\varepsilon}{\pi}}=\rho_k\lim_{\varepsilon\to0}\psi_k\left(\pm(w-\varepsilon),s_2\right)=\\&=\pm\sum_{m=0}^{M}\sum_{n=0}^{N}c_2^{mn}U_m(\pm1)\sqrt{1-(s_2/h)^2}U_n(s_2/h)\lim_{\varepsilon\to0}\sqrt{\frac{2\varepsilon}{w}}\end{aligned} \tag{61}$$

hence,

$$K_{\mathrm{I}}(\pm w,s_2)=\frac{E}{4(1-\nu^2)}\sqrt{\frac{\pi}{w}}\sum_{m=0}^{M}\sum_{n=0}^{N}\left(c_3^{mn}\cos\frac{w}{R}\pm c_1^{mn}\sin\frac{w}{R}\right)U_m(\pm1)\sqrt{1-(s_2/h)^2}U_n(s_2/h) \tag{62a}$$

$$K_{\mathrm{II}}(\pm w,s_2)=\frac{E}{4\left(1-\nu^2\right)}\sqrt{\frac{\pi}{w}}\sum_{m=0}^{M}\sum_{n=0}^{N}\left(c_1^{mn}\cos\frac{w}{R}\mp c_3^{mn}\sin\frac{w}{R}\right)U_m(\pm1)\sqrt{1-(s_2/h)^2}U_n(s_2/h) \tag{62b}$$

$$K_{\mathrm{III}}\left(\pm w, s_2\right) = \pm \frac{E}{4\left(1+\nu\right)}\sqrt{\frac{\pi}{w}} \sum_{m=0}^{M} \sum_{n=0}^{N} c_2^{mn} U_m(\pm 1)\sqrt{1-(s_2/h)^2}\, U_n(s_2/h) \tag{62c}$$

while on the crack front BC:

$$\begin{aligned} n_k(s_1,\pm h) \lim_{\varepsilon\to 0} \Delta u_k\left(R\sin\frac{s_1}{R}, \pm(h-\varepsilon), R\cos\frac{s_1}{R}\right) &= 4K_{\mathrm{I}}\frac{1-\nu^2}{E}\lim_{\varepsilon\to 0}\sqrt{\frac{2\varepsilon}{\pi}} = n_k \lim_{\varepsilon\to 0}\psi_k(s_1,\pm(h-\varepsilon)) = \\ = \left(\delta_{k1}\sin\frac{s_1}{R} + \delta_{k3}\cos\frac{s_1}{R}\right) &\sum_{m=0}^{M}\sum_{n=0}^{N} c_k^{mn}\sqrt{1-(s_1/w)^2}\, U_m(s_1/w) U_n(\pm 1)\lim_{\varepsilon\to 0}\sqrt{\frac{2\varepsilon}{h}} \end{aligned} \tag{63a}$$

$$\begin{aligned} \tau_k(s_1,\pm h) \lim_{\varepsilon\to 0} \Delta u_k\left(R\sin\frac{s_1}{R}, \pm(h-\varepsilon), R\cos\frac{s_1}{R}\right) &= 4K_{\mathrm{II}}\frac{1-\nu^2}{E}\lim_{\varepsilon\to 0}\sqrt{\frac{2\varepsilon}{\pi}} = \tau_k \lim_{\varepsilon\to 0}\psi_k(s_1,\pm(h-\varepsilon)) = \\ = \pm \sum_{m=0}^{M}\sum_{n=0}^{N} &c_2^{mn}\sqrt{1-(s_1/w)^2}\, U_m(s_1/w) U_n(\pm 1)\lim_{\varepsilon\to 0}\sqrt{\frac{2\varepsilon}{h}} \end{aligned} \tag{63b}$$

$$\begin{aligned} \rho_k(s_1,\pm h) \lim_{\varepsilon\to 0} \Delta u_k\left(R\sin\frac{s_1}{R}, \pm(h-\varepsilon), R\cos\frac{s_1}{R}\right) &= 4K_{\mathrm{III}}\frac{1+\nu}{E}\lim_{\varepsilon\to 0}\sqrt{\frac{2\varepsilon}{\pi}} = \rho_k \lim_{\varepsilon\to 0}\psi_k(s_1,\pm(h-\varepsilon)) = \\ = \mp\left(\delta_{i1}\cos\frac{s_1}{R} - \delta_{i3}\sin\frac{s_1}{R}\right) &\sum_{m=0}^{M}\sum_{n=0}^{N} c_k^{mn}\sqrt{1-(s_1/w)^2}\, U_m(s_1/w) U_n(\pm 1)\lim_{\varepsilon\to 0}\sqrt{\frac{2\varepsilon}{h}} \end{aligned} \tag{63c}$$

hence,

$$K_{\mathrm{I}}(s_1,\pm h) = \frac{E}{4\left(1-\nu^2\right)}\sqrt{\frac{\pi}{h}} \sum_{m=0}^{M}\sum_{n=0}^{N}\left(c_1^{mn}\sin\frac{s_1}{R} + c_3^{mn}\cos\frac{s_1}{R}\right)\sqrt{1-(s_1/w)^2}\, U_m(s_1/w) U_n(\pm 1) \tag{64a}$$

$$K_{\mathrm{II}}(s_1,\pm h) = \pm\frac{E}{4\left(1-\nu^2\right)}\sqrt{\frac{\pi}{h}} \sum_{m=0}^{M}\sum_{n=0}^{N} c_2^{mn}\sqrt{1-(s_1/w)^2}\, U_m(s_1/w) U_n(\pm 1) \tag{64b}$$

$$K_{\mathrm{III}}(s_1,\pm h) = \pm\frac{E}{4\left(1+\nu\right)}\sqrt{\frac{\pi}{h}} \sum_{m=0}^{M}\sum_{n=0}^{N}\left(c_3^{mn}\sin\frac{s_1}{R} - c_1^{mn}\cos\frac{s_1}{R}\right)\sqrt{1-(s_1/w)^2}\, U_m(s_1/w) U_n(\pm 1) \tag{64c}$$

Now, we give the expression for the stress tensor components in the local coordinate system at the point **x** on the crack surface. The directions of axes of the local coordinate system are given by vectors $\left(\boldsymbol{\tau},\boldsymbol{\rho},\mathbf{n}\right)$ with $n_i(\mathbf{x}) = \delta_{i1}\sin\frac{s_1}{R} + \delta_{i3}\cos\frac{s_1}{R}$, $\tau_i(\mathbf{x}) = \delta_{i1}\cos\frac{s_1}{R} - \delta_{i3}\sin\frac{s_1}{R}$, $\rho_i(\mathbf{x}) = \delta_{i2}$. Then, one can find easily

$$\sigma_{\tau\tau} = \tau_i\tau_k\sigma_{ik} = \sigma_{11}\cos^2\frac{s_1}{R} - \sigma_{13}\sin\frac{2s_1}{R} + \sigma_{33}\sin^2\frac{s_1}{R}$$

$$\sigma_{\tau\rho} = \tau_i\rho_k\sigma_{ik} = \sigma_{12}\cos\frac{s_1}{R} - \sigma_{32}\sin\frac{s_1}{R}, \sigma_{\rho\rho} = \rho_i\rho_k\sigma_{ik} = \sigma_{22}, \sigma_{\rho n} = \rho_i n_k\sigma_{ik} = \sigma_{12}\sin\frac{s_1}{R} + \sigma_{23}\cos\frac{s_1}{R},$$

$$\sigma_{\tau n} = \tau_i n_k\sigma_{ik} = \left(\sigma_{11}-\sigma_{33}\right)\frac{1}{2}\sin\frac{2s_1}{R} + \sigma_{13}\cos\frac{2s_1}{R} \tag{65}$$

$$\sigma_{nn} = n_i n_k \sigma_{ik} = \sigma_{11} \sin^2 \frac{s_1}{R} + \sigma_{13} \sin \frac{2s_1}{R} + \sigma_{33} \cos^2 \frac{s_1}{R}.$$

6. Numerical examples

6.1. A flat elliptical crack

We consider an elliptic crack subjected to uniform distributed pressure load σ_0 on the surface. Poisson's ratio $\nu = 0.3$ and Young's modulus is one unit. Maximum numbers of Chebyshev polynomials M and N are selected as 6 and 9 respectively. The numerical solutions of the stress intensity factor normalized to $\sigma_0 \frac{2}{\pi}\sqrt{\pi a}$ are given in Figure 11 versus the ratio b/a and angle φ in elliptic coordinates. We find that two normal stresses σ_{11}/σ_0 and σ_{22}/σ_0 are constants everywhere on the crack surface as shown in Table 2 and Table 3. In order to validate the accuracy of the numerical results, a cube with a centered embedded elliptic crack is considered with FEM simulation (ABAQUS) complemented with 690,319 C3D10 second-order tetrahedral elements. The length of the edge is five times of the semi-major axis *a*. The effect of the side on stress is then entirely neglected. The *T*-stresses by FEM and BIEM are plotted in Figure 12, while $b/a = 0.5$, varying with Poison's ratio with excellent agreement. We find $\sigma_{11}^* + \sigma_{22}^* = -(1+2\nu)\sigma_0$ and the relationship between normal stresses and Poisson's ratio ν is linear. The normal stresses are approximated, by curve fitting, as

$$\begin{aligned} \sigma_{11}^*/\sigma_0 &= -\frac{\beta}{2} + (\beta - 2)\nu, \\ \sigma_{22}^*/\sigma_0 &= \frac{(\beta-2)}{2} - \beta\nu, \end{aligned} \qquad b/a \le 1 \tag{66}$$

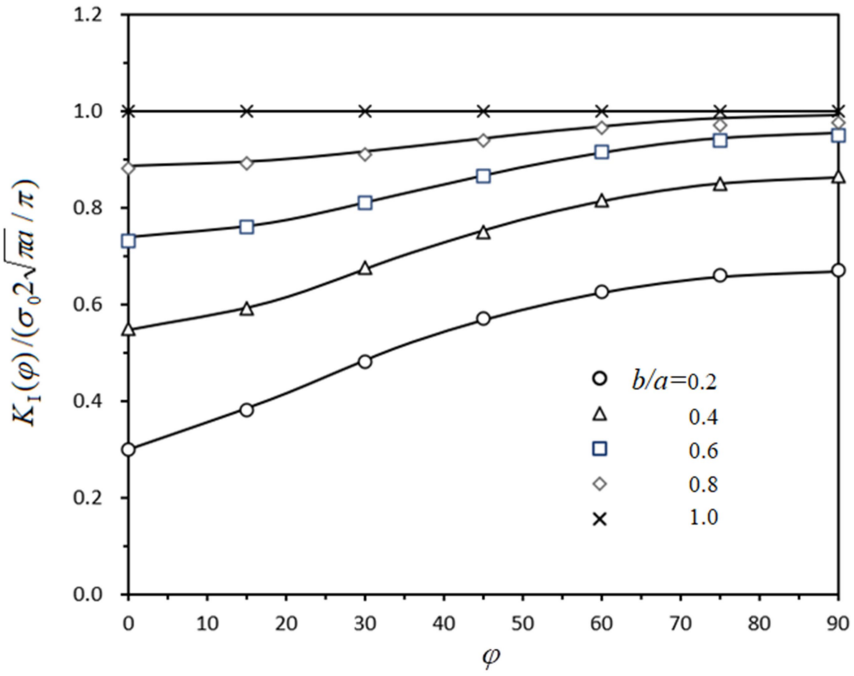

Figure 11. Normalized stress intensity factor $K_I(\varphi)/(\sigma_0 2\sqrt{\pi a}/\pi)$ versus the ratio of b/a.

where $\beta = b/a$. For a penny-shaped crack, $\beta = 1$, $T_{11} = T_{22} = -\frac{1+2\nu}{2}\sigma_0$, which is the same as analytical solution obtained by Wang [37]. As two normal stress σ_{11} and σ_{22} are constants, *T*-stress T_{11} at the points *A* and *B* are σ_{11}^* and σ_{22}^* respectively. In addition, we determine *T*-stress, along the crack front, by

$$T_{11} = \sigma_{11}^* n_1^2 + \sigma_{22}^* n_2^2 \ , \tag{67}$$

where n_1 and n_2 denote the outward normal shown in Figure 10(b). Consider the computational accuracy and efficiency, high convergent and accurate solutions of DDM for rectangular flat crack are illustrated both in Table 1 and Figure 7. Although the numerical results by the FEM are compared in Figure 12 with excellent agreement, the efficiency of the DDM with the Chebyshev polynomial interpolation is not easy to be concluded as the ABAQUS (FEM) is a commercial package running on the PC and DDM of 3D is implemented and coded in FORTRAN.

Table 2. Normalized *T*-Stress σ_{11}^{*}/σ_0 in the domain.

	b/a=0.1	0.2	0.3	0.4	0.5	0.6	0.7	0.8	0.9	1
0	-0.0253	-0.0786	-0.1400	-0.2024	-0.2614	-0.3180	-0.3699	-0.4175	-0.4607	-0.4999
0.1	-0.2202	-0.2629	-0.3120	-0.3619	-0.4091	-0.4544	-0.4960	-0.5340	-0.5686	-0.6000
0.2	-0.4152	-0.4472	-0.4840	-0.5214	-0.5569	-0.5908	-0.6220	-0.6505	-0.6764	-0.7000
0.3	-0.6101	-0.6315	-0.6560	-0.6810	-0.7046	-0.7272	-0.7480	-0.7670	-0.7843	-0.8000
0.4	-0.8051	-0.8157	-0.8280	-0.8405	-0.8523	-0.8636	-0.8740	-0.8835	-0.8921	-0.9000
0.5	-1.0000	-1.0000	-1.0000	-1.0000	-1.0000	-1.0000	-1.0000	-1.0000	-1.0000	-1.0000

Table 3. Normalized *T*-Stress σ_{22}^{*}/σ_0 in the domain.

	b/a=0.1	0.2	0.3	0.4	0.5	0.6	0.7	0.8	0.9	1
0	-0.9747	-0.9214	-0.8600	-0.7976	-0.7386	-0.6820	-0.6301	-0.5825	-0.5393	-0.5001
0.1	-0.9798	-0.9371	-0.8880	-0.8381	-0.7909	-0.7456	-0.7040	-0.6660	-0.6314	-0.6000
0.2	-0.9848	-0.9528	-0.9160	-0.8786	-0.8431	-0.8092	-0.7780	-0.7495	-0.7236	-0.7000
0.3	-0.9899	-0.9685	-0.9440	-0.9190	-0.8954	-0.8728	-0.8520	-0.8330	-0.8157	-0.8000
0.4	-0.9949	-0.9843	-0.9720	-0.9595	-0.9477	-0.9364	-0.9260	-0.9165	-0.9079	-0.9000
0.5	-1.0000	-1.0000	-1.0000	-1.0000	-1.0000	-1.0000	-1.0000	-1.0000	-1.0000	-1.0000

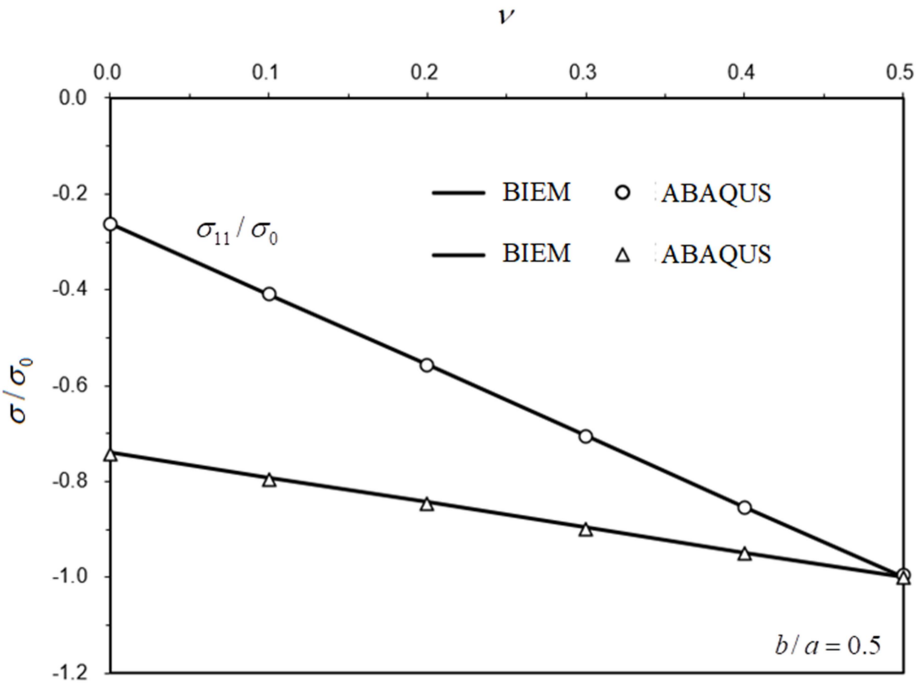

Figure 12. Normal stresses σ_{11}/σ_0 and σ_{22}/σ_0 versus the Poisson ratio and b/a.

6.2. Rectangular crack on a cylinder

Consider a rectangular crack $(w\times h)$ on a cylinder surface of radius R subjected to a remote tensile load shown in Figure 10(a). A remote tensile load σ_0 along axis x_3 is shown in Figure 10(a) and Poisson's ratio $\nu = 0.3$. Maximum numbers of the Chebyshev polynomials M and N are 6 and 9 respectively with angle $\alpha_0 = \pi/4$, then $w = \pi R/4, R = \sqrt{2}a$. The results of normalized stress intensity factor $K_{\mathrm{I}}(s_2)/\sigma_0\sqrt{\pi a}$ along the crack front AC and $K_{\mathrm{I}}(s_1)/\sigma_0\sqrt{\pi h}$ along BC vs the ratio of h/w are shown in Figures 13 and 14. We observe that maximum mode I and mode II stress intensity factors are at the center points A and B. Furthermore, the normalized shearing mode stress intensity factor $K_{\mathrm{II}}(s_2)/\sigma_0\sqrt{\pi a}$ along the crack front AC and tearing mode stress intensity factor $K_{\mathrm{III}}(s_1)/\sigma_0\sqrt{\pi h}$ along BC are presented in Figures 15 and 16 respectively. When $h/a = 5$, we noticed that the numerical normalized mode I and mode II intensity factors are 0.5476 and 0.6131, which agree very well with that for a 2D circular arc crack under same tensile load, i.e. the analytical solutions 0.55 and 0.61 respectively from stress intensity factors handbook [40]. However, mode III maximum stress intensity factor $K_{\mathrm{III}}(s_1)/\sigma_0\sqrt{\pi h}$ is observed in the region of $(0.7 < s_2/h < 0.8)$.

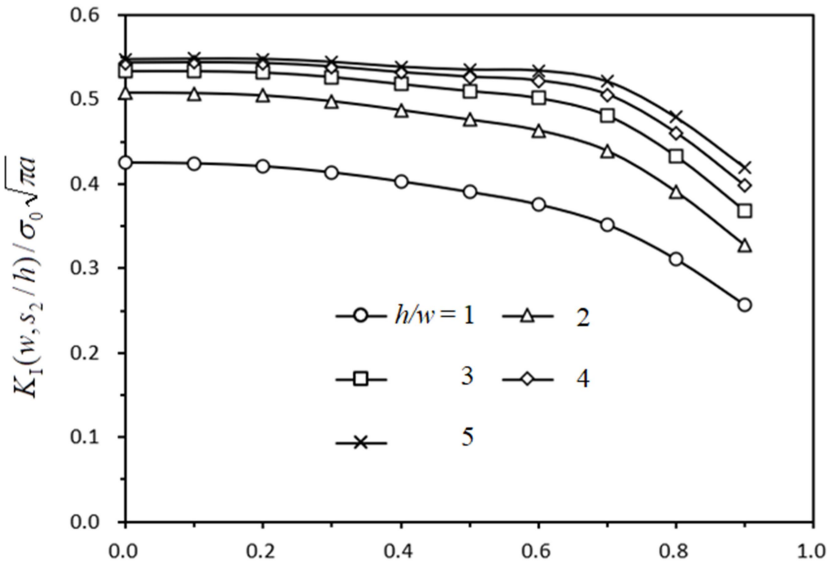

Figure 13. Normalized stress intensity factor $K_{\mathrm{I}}(s_2)/\sigma_0\sqrt{\pi a}$ along the crack front AC.

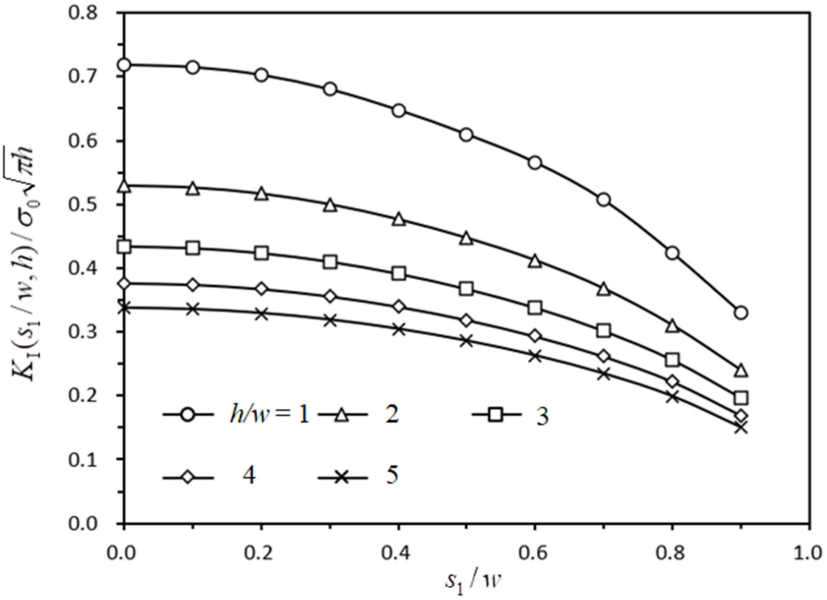

Figure 14. Normalized stress intensity factor $K_I(s_1)/\sigma_0\sqrt{\pi h}$ along the crack front BC.

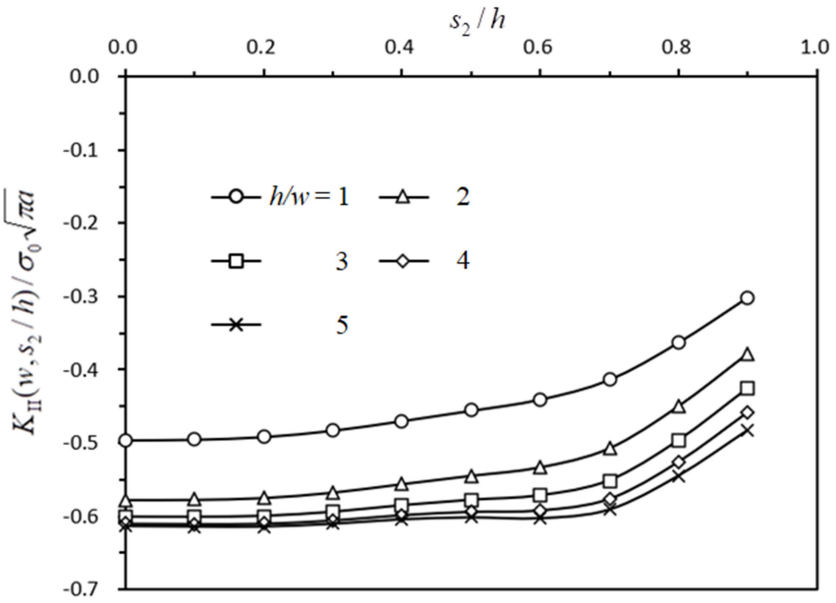

Figure 15. Normalized stress intensity factor $K_{II}(s_2)/\sigma\sqrt{\pi a}$ along the crack front AC.

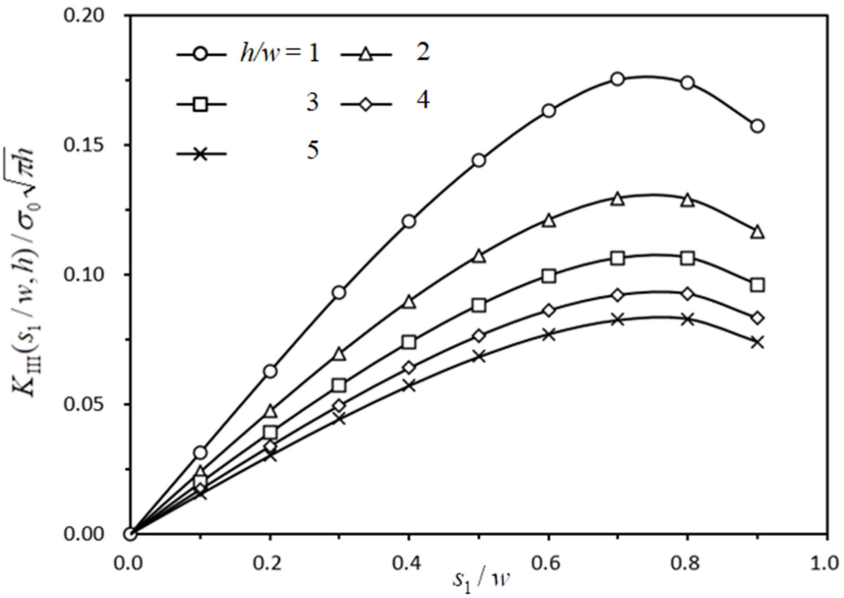

Figure 16. Normalized stress intensity factor $K_{III}(s_1)/\sigma_0\sqrt{\pi h}$ along the crack front BC.

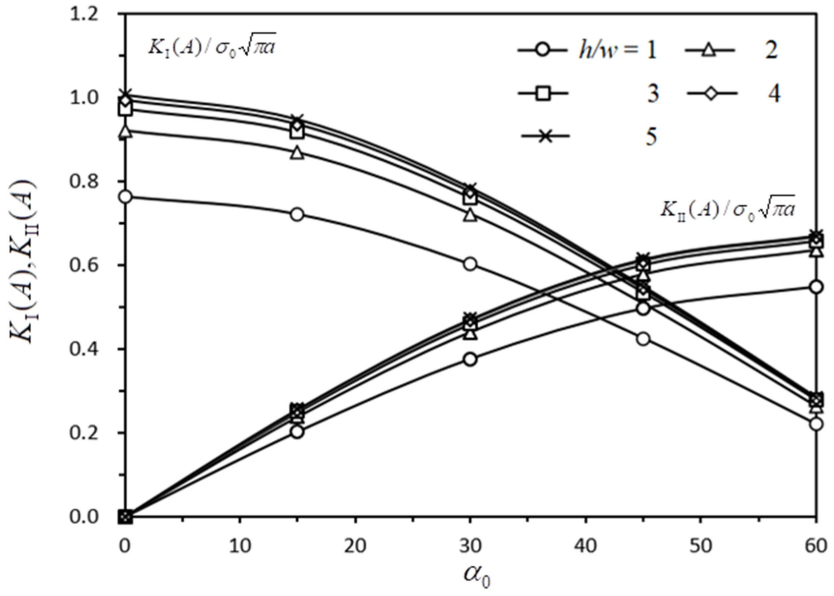

Figure 17. Maximum stress intensity factor at the crack tip A.

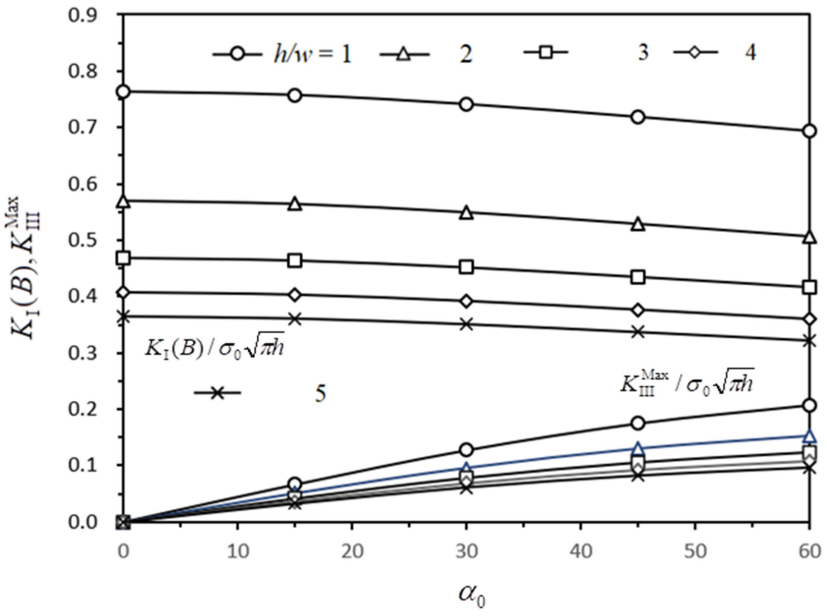

Figure 18. Stress intensity factor $K_I(B)/\sqrt{\pi h}$ at crack tip B and maximum $K_{III}/\sqrt{\pi h}$ along BC.

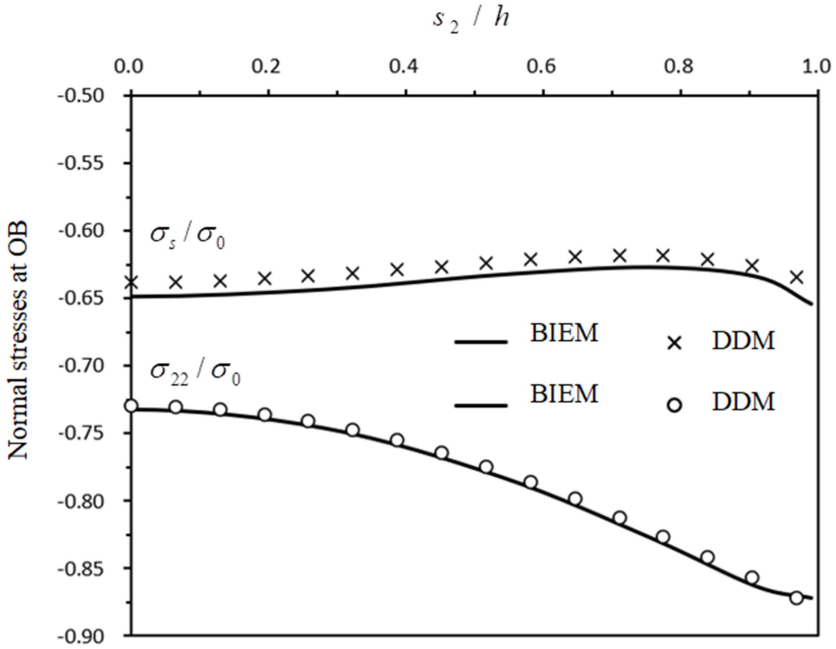

Figure 19. Normal stress distributions $\sigma_s(s_2)/\sigma_0$ and $\sigma_{22}(s_2)/\sigma_0$ along OB.

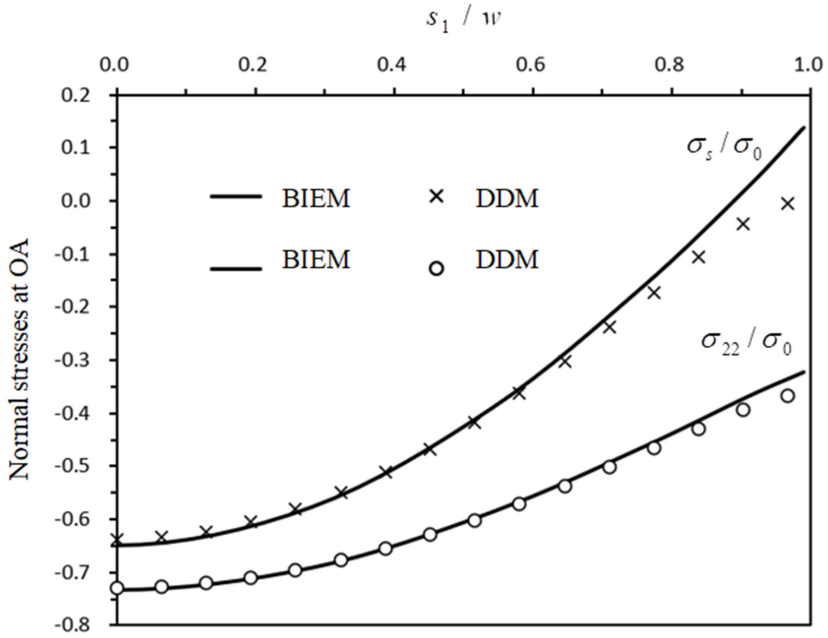

Figure 20. Normal stress distributions $\sigma_s(s_1)/\sigma_0$ and $\sigma_{22}(s_1)/\sigma_0$ along OA.

In addition, we present maximum stress intensity factors versus the angle of α and the ratio of h/w in Figures 17 and 18. Finally, two normal stress distributions along OA and OB on the crack surface are presented in Figures 19 and 20 to show the *T*-stresses at crack front points A and B. The numerical results given by the discontinuity displacement method [42] are also shown in the same figure for comparison. For general shape of crack surface, mapping technique can be applied. In the mapped domain, the shape of the crack surface becomes a square or a circular configuration. The displacement discontinuities are interpolated using two sets of the Chebyshev polynomials.

7. Conclusions

In this paper, we have presented the boundary integral equations method (BIEM) to analyse 3D fracture problems. Computational procedure for a flat rectangular, elliptic cracks and a curved rectangular crack on a cylindrical surface in an infinite domain are implemented to demonstrate the degrees of convergence and accuracy with BIEM. The spatial approximation of displacement discontinuities by using Chebyshev polynomials of the second kind enables us to solve the considered boundary value problems numerically with reliable modelling of singularities near the

crack front as well as evaluation of the stress intensity factors and T-stresses. Three-dimensional finite element analysis and the displacement discontinuity method are fulfilled to verify the numerical solutions by BIEM. It is found that *T*-stress strongly depends on the Poisson ratio of material and configuration of the crack surface. It has been observed that the normal stresses are constants on the elliptical crack surface in the principal axis coordinate and linearly dependent on the Poisson ratio. The approximation formulas for two normal stresses along principal axis are proposed for fast calculation for *T*-stresses. Numerical examples demonstrate the accuracy and efficiency of the BIEM for 3D fracture problems. These elastic *T*-stresses are suitable for the analysis of constraint effects for engineering components with embedded cracks. We believe that BIEM can be extended to 3D continuously nonhomogeneous solids with cracks under static and dynamic loadings. For hexagon shape crack, SIF and T-stresses can be obtained by superposition principle with sub-region and mapping methods used in FEM/BEM.

Acknowledgment

The authors acknowledge the support of the Slovak Science and Technology Assistance Agency registered under number APVV-18-0004, VEGA-2/0061/20.

References

[1] Du ZZ, Hancock JW. 1991. The effect of nonsingular stresses on crack tip constraint. *J. Mech Phys Solids* **39**: 555-567.

[2] Larsson SG, Carlson AJ. 1973. Influence of non-singular stress terms and specimen geometry on small scale yielding at crack tips in elastic–plastic materials. *J Mech Phys Solids* **21**:263-277.

[3] O'Dowd NP, Shih C, Dodds R. 1995. The role of geometry and crack growth on constraint and implications for ductile/brittle fracture. *Am Soc Test Mater* **2**:134-159.

[4] Cotterell B, Rice J R. 1980. Slightly curved or kinked cracks. *Int. J. Fruct*. **16**, 155-169.

[5] Gupta M, Alderliesten RC, Benedictus R. 2015. A review of T-stress and its effects in fracture mechanics. *Engineering Fracture Mechanics* **134**:218–241.

[6] Fett T. 2008. *Stress intensity factors, T-stresses, weight functions.* Karlsruhe, Germany: University of Karlsruhe.

[7] Nakamura T, Parks DM. 1992. Determination of elastic T -stress along three-dimensional crack fronts using an interaction integral. *Int J Solids Struct* **29**:1597–611.

[8] Nakamura, T. and Parks, D. M. 1989. Antisymmetrical 3-D stress field near the crack front of a thin elastic plate. *Int. J. Solid7 Structures* **25**: 141 l-1426.

[9] Betti E. 1972. Teori dell elasticita, II Nuovo Cimento, 7-10.

[10] Somigliana C. 1886. Sopra I'equilibrio di un corpo elastico isotropo, Il Nuovo Cienmento, 17-19.

[11] Muskhelishvili NI. 1953. *Some Basic Problems of the Mathematical Theory of Elasticity*. Noordhoff, Leyden.

[12] Kupradze VD. 1965. *Potential Methods in the Theory of Elasticity*, Israel Prog. Sci. Trans.

[13] Massonnet CE. 1965. Numerical use of integral procedures. In *Stress Analysis*, Chapter 10, 98-235, Wiley, London.

[14] Rizzo FJ. 1967. An integral equation approach to boundary value problems of classical elastostatics. *Quartely Journal of Applied Mathematics* **25:** 83-95.

[15] Cruse TA. 1969. Numerical solutions in three-dimensional elastostatics. *International Journal of Solids and Structures* **5:** 1259-1274.

[16] Hong HK, Chen JT. 1988. Generality and special cases of dual integral equations of elasticity. J Chin Soc Mech Eng; 9:1–9.

[17] Hong HK, Chen JT. 1988. Derivations of integral equations of elasticity. J Eng Mech; 114:1028–44.

[18] Portela A, Aliabadi MH, Rooke DP. 1991. Efficient boundary element analysis of sharp notched plates. *International.Journal for Numerical Methods in Engineering* **32:** 445-470.

[19] Mi Y, Aliabadi MH. 1992. Dual boundary element method for three dimensional fracture mechanics analysis. *Engineering Analysis* **10**(2): 161-171.

[20] Aliabadi MH. Boundary element formulations in fracture mechanics. *Appl Mech Rev* 1997; **50**: 83–96.

[21] Chen JT, Hong HK. Review of dual boundary element methods with emphasis on hypersingular integrals and divergent series. *Appl Mech Rev* 1999; **52**:17–33.

[22] P.H. Wen, Y.D. Tang, J. Sladek, V. Sladek. 2021. BEM analysis for curved cracks. *Engineering Analysis With Boundary Elements* **127**: 91-201.

[23] Crouch SL, Starfield AM. 1983. *Boundary Elements in Solid Mechanics*, George Allen and Unwin, London.

[24] Wen PH. 1991. The calculation of SIF considering the effects of arc crack surface contact and friction under uniaxial tension and pressure. *Eng. Fract. Mech*. **36** (4): 651-660.

[25] Wen PH, Fan TH, Yuan XG. 1992. A coupled method for evaluating stress intensity factor in the problems of crack orthotropic plane. *J. Cent. South Inst. Min. Metall*. **24** (4).

[26] Wen PH, Fan H. 1994. The discontinuity displacement method applied to three-dimensional co-planar crack problem for any boundary value condition. *Eng. Fract. Mech*. **48** (5): 505-517.

[27] Sladek J, Sladek V. 1997. Computation of thermoelastoplastic stresses in crack problems by the BEM. *Int J Fract* 83(4):359-78.

[28] Sladek J, Sladek V. 1997. Evaluation of T-stresses and stress intensity factors in stationary thermoelasticity by the conservation integral method. *Int J Fract.* **86**(3):199-219.

[29] Sladek J, Sladek V. 1997. Evaluations of the T-stress for interface cracks by the boundary element method. *Eng Fract Mech* **56**(6):813-25.

[30] Wen PH, Cao P, Korakianitis T. 2014. Finite Block Method in elasticity. *Engineering Analysis With Boundary Elements* **46**: 116-125.

[31] Li M, Meng LX, Hinneh P, Wen PH. 2016. Finite block method for interface cracks. *Engineering Fracture Mechanics* **156**: 25-40.

[32] Huang T, Yang JJ, Jin J, Wen PH, Aliabadi MH. 2018. Evaluation of stress intensity factors and *T*-stress by finite block method: Static and dynamic. *Theoretical and Applied Fracture Mechanic.* **93**,222-232.

[33] Williamss ML. 1959. The stresses around a fault or crack in dissimilar media, *Bull. Seismol. Soc. Amer*. **49**: 199-204.

[34] Deng X. 1994. The asymptotic structure of transient elastodynamic fields at the tip of a stationary crack. *Proc R Soc London A* **446**:1-13.

[35] Wang YY, Parks DM. 1992. Evaluation of the elastic T -stress in surface cracked plates using the line-spring method. *Int J Fract.* **56**:25–40.

[36] Zhao LG, Tong J, Byrne J. 2001. Stress intensity factor and elastic T -stress for corner cracks. *Int J Fract.* **109**:209–25.

[37] Wang X. 2003. Elastic T -stress solutions for semi-elliptical surface cracks in finite thickness plates. *Engng Fract Mech* **70**:731–56

[38] Wang X. 2004. Elastic T -stress solutions for penny-shaped cracks under tension and bending, *Engineering Fracture Mechanics* **71:** 2283–2298.

[39] Aliabadi MH. 2002. *The Boundary Element Method*, Vol 2: Applications in Solids and Structures. New York:Wiley.

[40] Murakami Y. 1986. *Stress Intensity Factors Handbook*, Pergamon Press.

[41] Rooke DP, Cartwright DJ. 1976. *Compendium of Stress Intensity Factors*, London, Her Majesty's Stationery Office.

[42] Wen PH. 1996. *Dynamic Fracture Mechanics: Displacement Discontinuity Method*. Computational Mechanics Publications, Southampton UK and Boston USA.

Appendix A

From Figure 9(a), we have collocation point ξ and integral field point P, with polar coordinates (ρ,θ) in local coordinate system centered at ξ

$$x_1(\xi)=at\cos\varphi,\ x_2(\xi)=bt\sin\varphi,\ t\le 1,\ 0\le\varphi\le 2\pi \tag{A1}$$

$$x_1(P)=x_1(\xi)+\rho\cos\theta,\ x_2(P)=x_2(\xi)+\rho\sin\theta,\ \rho\in[0,\rho(\theta)],\ \theta\in[0,2\pi]. \tag{A2}$$

If P lies on the crack front, $\rho=\rho(\theta)$. As the coordinates along the crack front satisfy following equation

$$\left(\frac{x_1(P)}{a}\right)^2+\left(\frac{x_2(P)}{b}\right)^2=1, \tag{A3}$$

then, we have

$$\left(\frac{\cos^2\theta}{a^2}+\frac{\sin^2\theta}{b^2}\right)\rho^2+2\left(\frac{\cos\theta}{a^2}x_1(\xi)+\frac{\sin\theta}{b^2}x_2(\xi)\right)\rho-(1-t^2)=0,\ 0\le\theta\le 2\pi\ . \tag{A4}$$

Thus, the distance of $\rho(\theta)$ can be obtained by

$$\rho(\theta)=\frac{\sqrt{\beta^2+\alpha\gamma}-\beta}{\alpha}, \tag{A5}$$

in which

$$\alpha=b^2\cos^2\theta+a^2\sin^2\theta,\ \beta=b^2x_1(\xi)\cos\theta+a^2x_2(\xi)\sin\theta,\ \gamma=(1-t^2)a^2b^2. \tag{A6}$$

In order to derive the unit outward vector $\mathbf{n}(\mathbf{x}^f)$ normal to the crack front at point $\mathbf{x}^f$ with coordinates $x_1^f = a\cos\varphi$, $x_2^f = b\sin\varphi$, we derive firstly the tangent vector $\boldsymbol{\tau}(\mathbf{x}^f)$ at this point. Apparently, $x_2^f = b\sqrt{1-(x_1^f/a)^2}$, $\frac{\tau_2}{\tau_1} \sim \frac{dx_2^f}{dx_1^f} = -\frac{b}{a}\frac{x_1^f}{a}\frac{1}{\sqrt{1-(x_1^f/a)^2}} = -\left(\frac{b}{a}\right)^2\frac{x_1^f}{x_2^f} = -\frac{b}{a}\frac{\cos\varphi}{\sin\varphi} =: \lambda$.

Hence, $\tau_2 = \lambda\tau_1$ and from the requirement $(\tau_1)^2 + (\tau_2)^2 = 1$, we obtain $\tau_1 = -1/\sqrt{1+\lambda^2}$, $\tau_2 = -\lambda/\sqrt{1+\lambda^2}$ and finally,

$$n_1 = \tau_2 = \frac{b\cos\varphi}{\sqrt{(a\sin\varphi)^2 + (b\cos\varphi)^2}}, \quad n_2 = -\tau_1 = \frac{a\sin\varphi}{\sqrt{(a\sin\varphi)^2 + (b\cos\varphi)^2}} \ . \tag{A7}$$

Appendix B

It is convenient to map the curved surface of crack into a flat rectangle as shown in Figure B1, when the natural coordinates (s_1, s_2) are expressed in terms of straight coordinates (η_1, η_2) as $s_1 = w\eta_1$ and $s_2 = h\eta_2$. Then, the parametric coordinates of the collocation point $\boldsymbol{\xi}$ with natural coordinates (s_1', s_2') are given by $\eta_1' = s_1'/w$, $\eta_2' = s_2'/h$. The real physical Cartesian coordinates of the collocation point $\boldsymbol{\xi} = (\xi_1, \xi_2, \xi_3)$ are given as

$$\xi_1 = R\sin\frac{w\eta_1'}{R}, \quad \xi_2 = h\eta_2', \quad \xi_3 = R\cos\frac{w\eta_1'}{R} \tag{B1}$$

and those for the integral field point $\mathbf{x} = (x_1, x_2, x_3)$ are given as

$$\begin{aligned} x_1(\xi,\zeta,\theta) &= R\sin\left(\frac{s_1}{R}\right) = R\sin\left(w\frac{\eta_1' + \zeta\cos\theta}{R}\right), \\ x_2(\xi,\zeta,\theta) &= s_2 = h(\eta_2' + \zeta\sin\theta), \\ x_3(\xi,\zeta,\theta) &= R\cos\left(\frac{s_1}{R}\right) = R\cos\left(w\frac{\eta_1' + \zeta\cos\theta}{R}\right), \end{aligned} \tag{B2}$$

where (ζ,θ) are polar coordinates in the parametric space with the origin of the polar coordinates being at the collocation point (η_1', η_2').

Now, $ds_1 ds_2 = wh\, d\eta_1 d\eta_2 = wh\zeta\, d\zeta\, d\theta$ and the distance between the collocation point and the field point is given as

$$r = \sqrt{(\xi_i - x_i)(\xi_i - x_i)} = \left[R^2 \left(\sin\frac{s_1}{R} - \sin\frac{s_1'}{R} \right)^2 + R^2 \left(\cos\frac{s_1}{R} - \cos\frac{s_1'}{R} \right)^2 + (h\zeta \sin\theta)^2 \right]^{1/2} = \zeta D(\zeta, \theta) \tag{B3}$$

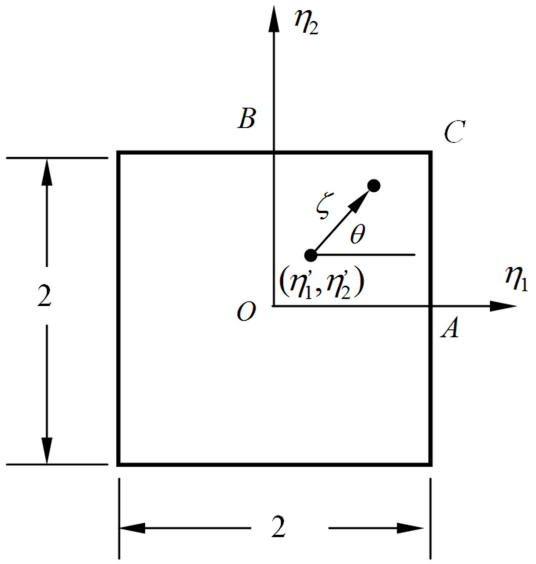

Figure B1. Mapped domain of the crack on cylindrical surface and parametric coordinate system.

with $D(\zeta, \theta) := \left[2\left(\frac{R}{\zeta}\right)^2 \left(1 - \cos\frac{\zeta w \cos\theta}{R} \right) + (h\sin\theta)^2 \right]^{1/2}$. It can be seen that

$$D(\zeta, \theta) = \left[(w\cos\theta)^2 + O(\zeta^2) + (h\sin\theta)^2 \right]^{1/2} = d(\theta) \left[1 + O(\zeta^2)/d^2 \right]^{1/2} = d(\theta) + O(\zeta^2) \tag{B4}$$

where $d(\theta) := \left[(w\cos\theta)^2 + (h\sin\theta)^2 \right]^{1/2}$. The outward unit normal vector on the crack surface at the field and collocation points are given as

$$n_i(s_1) = \delta_{i1} \sin\left(\frac{s_1}{R}\right) + \delta_{i3} \cos\left(\frac{s_1}{R}\right), n_i(s_1') = n_i(s_1)\big|_{\zeta=0} \tag{B5}$$

hence,

$$n_i(s_1) = n_i^{(0)} + \zeta n_i^{(1)} + v_i(s_1', \zeta, \theta) \ , \tag{B6}$$

with

$$n_i^{(0)} = n_i(s_1') \ , \ n_1^{(1)}(s_1', \theta) = \frac{w\cos\theta}{R} n_3^{(0)} \ ,$$

$$v_1(s_1', \zeta, \theta) = 2n_3^{(0)}\left(\sin\bar{\zeta}\cos\bar{\zeta} - \bar{\zeta}\right) - 2n_1^{(0)}\sin^2\bar{\zeta} \sim O\left(\zeta^2\right), n_3^{(1)}(s_1', \theta) = -\frac{w\cos\theta}{R} n_1^{(0)} \ ,$$

$$v_3(s_1', \zeta, \theta) = 2n_1^{(0)}\left(\bar{\zeta} - \sin\bar{\zeta}\cos\bar{\zeta}\right) - 2n_3^{(0)}\sin^2\bar{\zeta} \sim O\left(\zeta^2\right), \quad \bar{\zeta} = \frac{\zeta w\cos\theta}{2R} .$$

Now, we have

$$r_1 = x_1 - \xi_1 = R\left[\sin\left(\frac{s_1}{R}\right) - \sin\left(\frac{s_1'}{R}\right)\right] = 2R\left(n_3^{(0)}\sin\bar{\zeta}\cos\bar{\zeta} - n_1^{(0)}\sin^2\bar{\zeta}\right) \ , \quad r_{,1} = \frac{r_1}{\zeta D(\zeta, \theta)} \ ,$$

$$r_2 = x_2 - \xi_2 = \zeta h\sin\theta \ , \quad r_{,2} = \frac{h\sin\theta}{D(\zeta, \theta)} , \tag{B7}$$

$$r_3 = x_3 - \xi_3 = R\left[\cos\left(\frac{s_1}{R}\right) - \cos\left(\frac{s_1'}{R}\right)\right] = -2R\left(n_1^{(0)}\sin\bar{\zeta}\cos\bar{\zeta} + n_3^{(0)}\sin^2\bar{\zeta}\right), \quad r_{,3} = \frac{r_3}{\zeta D(\zeta, \theta)} .$$

Apparently, consider $\lim_{\zeta\to 0} r_{,i} = r_{,i}^{(0)}$, with

$$r_{,1}^{(0)} = \frac{w\cos\theta}{d(\theta)} n_3^{(0)} , \quad r_{,2}^{(0)} = \frac{h\sin\theta}{d(\theta)} , \quad r_{,3}^{(0)} = -\frac{w\cos\theta}{d(\theta)} n_1^{(0)} \tag{B8}$$

and

$$r_{,i}(s_1', \zeta, \theta) = r_{,i}^{(0)}(s_1', \theta) + \zeta r_{,i}^{(1)}(s_1', \theta) + \rho_i(s_1', \zeta, \theta) , \tag{B9}$$

we have

$$r_1^{(1)} = -\frac{(w\cos\theta)^2}{2Rd} n_1^{(0)} , \quad \rho_1 = \frac{w\cos\theta}{d}\left[\left(\frac{d}{D}\frac{\sin\bar{\zeta}}{\bar{\zeta}}\cos\bar{\zeta} - 1\right)n_3^{(0)} - n_1^{(0)}\left(\frac{d}{D}\frac{\sin\bar{\zeta}}{\bar{\zeta}}\sin\bar{\zeta} - \bar{\zeta}\right)\right] \sim O\left(\zeta^2\right)$$

$$r_2^{(1)} = 0 , \quad \rho_2 = \frac{h\sin\theta}{Dd}(d - D) \sim O\left(\zeta^2\right)$$

$$r_1^{(1)} = -\frac{(w\cos\theta)^2}{2Rd} n_3^{(0)}, \quad \rho_3 = \frac{w\cos\theta}{d}\left[\left(1-\frac{d}{D}\frac{\sin\bar{\zeta}}{\bar{\zeta}}\cos\bar{\zeta}\right)n_1^{(0)} - n_3^{(0)}\left(\frac{d}{D}\frac{\sin\bar{\zeta}}{\bar{\zeta}}\sin\bar{\zeta}-\bar{\zeta}\right)\right] \sim O\left(\zeta^2\right).$$

The singular behavior of the kernel $S_{ijk}^*(\boldsymbol{\xi},\mathbf{x})$ can be extracted as ζ^{-3}, since

$$S_{ijk}^*(\boldsymbol{\xi},\mathbf{x}) = \zeta^{-3}\Sigma_{ijk}(s_1',s_2',\zeta,\theta), \quad \Sigma_{ijk}(s_1',s_2',\zeta,\theta) = \frac{E}{8\pi(1-\nu^2)D^3(\zeta,\theta)} R_{ijk}(s_1',s_2',\zeta,\theta) \sim O(\zeta^0)$$

$$R_{ijk}(s_1',s_2',\zeta,\theta) := 3r_{,m}n_m\left[(1-2\nu)\delta_{ij}r_{,k} + \nu\left(\delta_{ik}r_{,j}+\delta_{jk}r_{,i}\right) - 5r_{,i}r_{,j}r_{,k}\right] +$$
$$+ 3\nu\left(n_i r_{,j} + n_j r_{,i}\right)r_{,k} + (1-2\nu)\left(3n_k r_{,i}r_{,j} + n_j\delta_{ik} + n_i\delta_{jk}\right) - (1-4\nu)n_k\delta_{ij}$$

Furthermore,

$$H_{mn}(s_1,s_2) := \sqrt{1-\left(\frac{s_1}{w}\right)^2}\,U_m\left(\frac{s_1}{w}\right)\sqrt{1-\left(\frac{s_2}{h}\right)^2}\,U_m\left(\frac{s_2}{h}\right) \to H_{mn}(s_1',s_2') \sim \mathrm{O}\left(\zeta^0\right) \text{ as } \zeta\to 0.$$

In order to evaluate the finite part integral in the integral equation (57)

$$A_{mnik}(s_1',s_2') = n_j(s_1') \oint\limits_{S^-} H_{mn}(s_1,s_2)S_{ijk}^*(\boldsymbol{\xi},\mathbf{x})ds_1ds_2 =$$
$$= whn_j(s_1') \int\limits_0^{2\pi}\int\limits_0^{\zeta(\theta)} \zeta^{-2}H_{mn}(s_1,s_2)\Sigma_{ijk}(s_1',s_2',\zeta,\theta)d\zeta d\theta \tag{B10}$$

it is appropriate to specify the asymptotic behavior of the integrand near the singular point (s_1',s_2'). Thus,

$$H_{mn}(s_1,s_2) = F_{mn}(s_1',s_2',\zeta,\theta) + H_{mn}^{(0)}(s_1',s_2') + \zeta H_{mn}^{(1)}(s_1',s_2',\theta) \tag{B11}$$
$$H_{mn}^{(0)}(s_1',s_2') := H_{mn}(s_1,s_2)\big|_{\zeta=0} = H_{mn}(s_1',s_2')$$

$$H_{mn}^{(1)}(s_1',s_2',\theta) := \left(\frac{\partial s_1}{\partial\zeta}\frac{\partial}{\partial s_1} + \frac{\partial s_2}{\partial\zeta}\frac{\partial}{\partial s_2}\right)H_{mn}(s_1,s_2)\Big|_{\zeta=0} = \left(w\cos\theta\frac{\partial}{\partial s_1} + h\sin\theta\frac{\partial}{\partial s_2}\right)H_{mn}(s_1,s_2)\Big|_{\zeta=0}$$

$$F_{mn}(s_1',s_2',\zeta,\theta) = H_{mn}(s_1,s_2) - \left[H_{mn}^{(0)}(s_1',s_2') + \zeta H_{mn}^{(1)}(s_1',s_2',\theta)\right] \sim O\left(\zeta^2\right)$$

$$\Sigma_{ijk}(s_1',s_2',\zeta,\theta) = \frac{E}{8\pi(1-\nu^2)}\left(\frac{1}{D^3(\zeta,\theta)} - \frac{1}{d^3(\theta)}\right)R_{ijk}(s_1',s_2',\zeta,\theta) + \frac{E}{8\pi(1-\nu^2)d^3(\theta)}R_{ijk}(s_1',s_2',\zeta,\theta) =$$
$$= \Sigma_{ijk}^{(2)}(s_1',s_2',\zeta,\theta) + \Sigma_{ijk}^{(0)}(s_1',s_2',\theta) + \zeta\,\Sigma_{ijk}^{(1)}(s_1',s_2',\theta) \tag{B12}$$

with

$$\Sigma_{ijk}^{(2)}(s_1',s_2',\zeta,\theta)=\frac{E}{8\pi(1-\nu^2)}\left\{\left(\frac{1}{D^3(\zeta,\theta)}-\frac{1}{d^3(\theta)}\right)R_{ijk}(s_1',s_2',\zeta,\theta)+\frac{1}{d^3(\theta)}R_{ijk}^{(2)}(s_1',s_2',\zeta,\theta)\right\}\sim O\left(\zeta^2\right)$$

$$\Sigma_{ijk}^{(0)}(s_1',s_2',\theta)=\frac{E}{8\pi(1-\nu^2)d^3(\theta)}R_{ijk}^{(0)}(s_1',s_2',\theta)\,,\quad \Sigma_{ijk}^{(1)}(s_1',s_2',\theta)=\frac{E}{8\pi(1-\nu^2)d^3(\theta)}R_{ijk}^{(1)}(s_1',s_2',\theta)$$

since

$$R_{ijk}(s_1',s_2',\zeta,\theta)=R_{ijk}^{(0)}(s_1',s_2',\theta)+\zeta R_{ijk}^{(1)}(s_1',s_2',\theta)+R_{ijk}^{(2)}(s_1',s_2',\zeta,\theta)$$

$$\begin{aligned}R_{ijk}^{(0)}(s_1',s_2',\theta)=3\left(r_{,m}n_m\right)^{(0)}&\left[(1-2\nu)\delta_{ij}r_{,k}^{(0)}+\nu\left(\delta_{ik}r_{,j}^{(0)}+\delta_{jk}r_{,i}^{(0)}\right)-5\left(r_{,i}r_{,j}r_{,k}\right)^{(0)}\right]+\\&+3\nu\left[\left(r_{,j}r_{,k}n_i\right)^{(0)}+\left(r_{,i}r_{,k}n_j\right)^{(0)}\right]+(1-2\nu)\left[3\left(r_{,i}r_{,j}n_k\right)^{(0)}+n_j^{(0)}\delta_{ik}+n_i^{(0)}\delta_{jk}\right]-(1-4\nu)n_k^{(0)}\delta_{ij}\end{aligned}$$

$$\begin{aligned}R_{ijk}^{(1)}(s_1',s_2',\theta)=3&\left[(1-2\nu)\delta_{ij}\left(r_{,k}r_{,m}n_m\right)^{(1)}+\nu\left(\delta_{ik}\left(r_{,j}r_{,m}n_m\right)^{(1)}+\delta_{jk}\left(r_{,i}r_{,m}n_m\right)^{(1)}\right)-5\left(r_{,i}r_{,j}r_{,k}r_{,m}n_m\right)^{(1)}\right]+\\&+3\nu\left[\left(r_{,j}r_{,k}n_i\right)^{(1)}+\left(r_{,i}r_{,k}n_j\right)^{(1)}\right]+(1-2\nu)\left[3\left(r_{,i}r_{,j}n_k\right)^{(1)}+n_j^{(1)}\delta_{ik}+n_i^{(1)}\delta_{jk}\right]-(1-4\nu)n_k^{(1)}\delta_{ij}\end{aligned}$$

$$\begin{aligned}R_{ijk}^{(2)}(s_1',s_2',\zeta,\theta)=3&\left[(1-2\nu)\delta_{ij}\left(r_{,k}r_{,m}n_m\right)^{(2)}+\nu\left(\delta_{ik}\left(r_{,j}r_{,m}n_m\right)^{(2)}+\delta_{jk}\left(r_{,i}r_{,m}n_m\right)^{(2)}\right)-5\left(r_{,i}r_{,j}r_{,k}r_{,m}n_m\right)^{(2)}\right]+\\&+3\nu\left[\left(r_{,j}r_{,k}n_i\right)^{(2)}+\left(r_{,i}r_{,k}n_j\right)^{(2)}\right]+(1-2\nu)\left[3\left(r_{,i}r_{,j}n_k\right)^{(2)}+\nu_j\delta_{ik}+\nu_i\delta_{jk}\right]-(1-4\nu)\nu_k\delta_{ij}\end{aligned}$$

in which

$$\begin{aligned}&\left(r_{,i}n_j\right)^{(0)}=r_{,i}^{(0)}n_j^{(0)}\,,\ \left(r_{,i}n_j\right)^{(1)}=r_{,i}^{(0)}n_j^{(1)}+r_{,i}^{(1)}n_j^{(0)}\,,\\&\left(r_{,i}n_j\right)^{(2)}=\zeta^2r_{,i}^{(1)}n_j^{(1)}+\nu_j\left(r_{,i}^{(0)}+\zeta r_{,i}^{(1)}+\rho_i\right)+\rho_i\left(n_j^{(0)}+\zeta n_j^{(1)}\right)\end{aligned}\qquad\text{(B13)}$$

$$\begin{aligned}&\left(r_{,i}r_{,j}\right)^{(0)}=r_{,i}^{(0)}r_{,j}^{(0)}\,,\ \left(r_{,i}r_{,j}\right)^{(1)}=r_{,i}^{(0)}r_{,j}^{(1)}+r_{,i}^{(1)}r_{,j}^{(0)}\\&\left(r_{,i}r_{,j}\right)^{(2)}=\zeta^2r_{,i}^{(1)}r_{,j}^{(1)}+\rho_j\left(r_{,i}^{(0)}+\zeta r_{,i}^{(1)}+\rho_i\right)+\rho_i\left(r_{,j}^{(0)}+\zeta r_{,j}^{(1)}\right)\end{aligned}$$

$$\begin{aligned}&\left(r_{,i}r_{,j}n_k\right)^{(0)}=r_{,i}^{(0)}r_{,j}^{(0)}n_k^{(0)}\,,\ \left(r_{,i}r_{,j}n_k\right)^{(1)}=n_k^{(0)}\left(r_{,i}r_{,j}\right)^{(1)}+n_k^{(1)}\left(r_{,i}r_{,j}\right)^{(0)}\,,\\&\left(r_{,i}r_{,j}n_k\right)^{(2)}=\zeta^2n_k^{(1)}\left(r_{,i}r_{,j}\right)^{(1)}+\nu_k\left(\left(r_{,i}r_{,j}\right)^{(0)}+\zeta\left(r_{,i}r_{,j}\right)^{(1)}+\left(r_{,i}r_{,j}\right)^{(2)}\right)+\left(n_k^{(0)}+\zeta n_k^{(1)}\right)\left(r_{,i}r_{,j}\right)^{(2)}\end{aligned}$$

$$\left(r_{,i}r_{,j}r_{,k}\right)^{(0)} = r_{,i}^{(0)}r_{,j}^{(0)}r_{,k}^{(0)},\ \left(r_{,i}r_{,j}r_{,k}\right)^{(1)} = r_{,k}^{(0)}\left(r_{,i}r_{,j}\right)^{(1)} + r_{,k}^{(1)}\left(r_{,i}r_{,j}\right)^{(0)}$$

$$\left(r_{,i}r_{,j}r_{,k}\right)^{(2)} = \zeta^2 r_{,k}^{(1)}\left(r_{,i}r_{,j}\right)^{(1)} + \rho_k\left(\left(r_{,i}r_{,j}\right)^{(0)} + \zeta\left(r_{,i}r_{,j}\right)^{(1)} + \left(r_{,i}r_{,j}\right)^{(2)}\right) + \left(r_{,k}^{(0)} + \zeta r_{,k}^{(1)}\right)\left(r_{,i}r_{,j}\right)^{(2)}$$

$$\left(r_{,i}r_{,j}r_{,k}r_{,m}n_m\right)^{(0)} = \left(r_{,i}r_{,j}r_{,k}\right)^{(0)}\left(r_{,m}n_m\right)^{(0)},\ \left(r_{,i}r_{,j}r_{,k}r_{,m}n_m\right)^{(1)} = \left(r_{,m}n_m\right)^{(0)}\left(r_{,i}r_{,j}r_{,k}\right)^{(1)} + \left(r_{,m}n_m\right)^{(1)}\left(r_{,i}r_{,j}r_{,k}\right)^{(0)}$$

$$\left(r_{,i}r_{,j}r_{,k}r_{,m}n_m\right)^{(2)} = \zeta^2\left(r_{,i}r_{,j}r_{,k}\right)^{(1)}\left(r_{,m}n_m\right)^{(1)} + \left(\left(r_{,m}n_m\right)^{(0)} + \zeta\left(r_{,m}n_m\right)^{(1)}\right)\left(r_{,j}r_{,m}n_m\right)^{(2)} +$$
$$+ \left(r_{,m}n_m\right)^{(2)}\left(\left(r_{,i}r_{,j}r_{,k}\right)^{(0)} + \zeta\left(r_{,i}r_{,j}r_{,k}\right)^{(1)} + \left(r_{,i}r_{,j}r_{,k}\right)^{(2)}\right)$$

Thus, the integrand in (B10) can be arranged as

$$\begin{aligned}
\zeta^{-2}H_{mn}(s_1,s_2)\Sigma_{ijk}(s_1',s_2',\zeta,\theta) &= \frac{1}{\zeta^2}\left[F_{mn}(s_1',s_2',\zeta,\theta) + H_{mn}^{(0)}(s_1',s_2') + \zeta H_{mn}^{(1)}(s_1',s_2',\theta)\right]\times \\
&\times\left[\Sigma_{ijk}^{(2)}(s_1',s_2',\zeta,\theta) + \Sigma_{ijk}^{(0)}(s_1',s_2',\theta) + \zeta\Sigma_{ijk}^{(1)}(s_1',s_2',\theta)\right] = \\
&= \frac{1}{\zeta^2}\left[F_{mn}\left(\Sigma_{ijk}^{(2)} + \Sigma_{ijk}^{(0)} + \zeta\Sigma_{ijk}^{(1)}\right) + \left(H_{mn}^{(0)} + \zeta H_{mn}^{(1)}\right)\Sigma_{ijk}^{(2)} + \zeta^2 H_{mn}^{(1)}\Sigma_{ijk}^{(1)}\right] + \\
&+ \frac{1}{\zeta^2}H_{mn}^{(0)}\Sigma_{ijk}^{(0)} + \frac{1}{\zeta}\left[H_{mn}^{(0)}\Sigma_{ijk}^{(1)} + H_{mn}^{(1)}\Sigma_{ijk}^{(0)}\right],
\end{aligned} \tag{B14}$$

and the finite part integral in (B10) is given by

$$\begin{aligned}
&A_{mnik}(s_1',s_2') = \\
&= whn_j(s_1')\int_0^{2\pi}\left\{\int_0^{\zeta(\theta)}\frac{1}{\zeta^2}\left[F_{mn}\left(\Sigma_{ijk}^{(2)} + \Sigma_{ijk}^{(0)} + \zeta\Sigma_{ijk}^{(1)}\right) + \left(H_{mn}^{(0)} + \zeta H_{mn}^{(1)}\right)\Sigma_{ijk}^{(2)} + \zeta^2 H_{mn}^{(1)}\Sigma_{ijk}^{(1)}\right]d\zeta - \right. \\
&\left. - \frac{1}{\zeta(\theta)}H_{mn}^{(0)}\Sigma_{ijk}^{(0)} + \left[H_{mn}^{(0)}\Sigma_{ijk}^{(1)} + H_{mn}^{(1)}\Sigma_{ijk}^{(0)}\right]\ln\zeta(\theta)\right\}d\theta.
\end{aligned} \tag{B15}$$